arXiv:1403.4505v2 [cond-mat.soft] 19 Nov 2014

Deriving fundamental measure theory from the virial series: Consistency with the zero-dimensional limit

Matthieu Marechal,[1] Stephan Korden,[2] and Klaus Mecke[1]

[1] *Institut für Theoretische Physik, Universität Erlangen-Nürnberg, Staudtstr. 7, 91058 Erlangen, Germany*
[2] *Institute of Technical Thermodynamics, RWTH Aachen University, Schinkelstraße 8, 52062 Aachen, Germany*

(Dated: February 28, 2022)

Fundamental measure theory (FMT) for hard particles has great potential for predicting the phase behavior of colloidal and nanometric shapes. The modern versions of FMT are usually derived from the zero-dimensional limit, a system of at most one particle confined in a collection of cavities in the limit that all cavities shrink to the size of the particle. In [Phys. Rev. E **85**, 041150 (2012)], a derivation from an approximated and resummed virial expansion was presented, whose result was not fully consistent with the FMT from the zero-dimensional limit. Here we improve upon this derivation and obtaining exactly the same FMT functional as was obtained earlier from the zero-dimensional limit. As a result, further improvements of FMT based on the virial expansion can now be formulated, some of which we suggest in the outlook.

PACS numbers: 05.20.Jj, 82.70.Dd

I. Introduction

Hard particles have been used as a reference model for molecules in most theoretical approaches. Moreover, recent progress [1] in synthesis techniques have allowed the manufacture of colloids and nano-particles of near arbitrary shape. Predicting the collective behavior of arbitrarily shaped particles provides a challenge for theory and simulations alike, if only because of the plethora of available shapes.

Density functional theory (DFT) [2] is a theory for equilibrium phase behavior of inhomogeneous many-particle systems. A DFT for mixtures of hard spheres, fundamental measure theory (FMT), was derived by Rosenfeld [3]. More recent versions are based on a different derivation by Tarazona and Rosenfeld[4] that demanded that the functional is exact in the so-called zero-dimensional limit: A collection of overlapping cavities which, as a whole, can contain at most one particle in the limit that each cavity shrinks to the size of the particle. We will refer to the functional that is exact for three cavities whose intersection is nonzero as the 0D-FMT functional. After some modifications [4–7] (see also Sec. VII C), the theory provides a good description of both the crystal and the high density fluid and accurately predicts the bulk freezing transition [8]. In addition, this latest DFT has been applied to inhomogeneous systems of hard spheres, such as a fluid around a hard spherical obstacle [7] and the fluid-solid interface [9].

Fundamental measure theory was also extended to (mixtures of) non-spherical hard particles by Rosenfeld [10] whose description lacked a stable nematic phase. This artifact of FMT was repaired [11, 12] by applying the Gauss-Bonnet theorem to the intersection between two particles [13], which appears in the lowest order in the excess free energy (with respect to that of the ideal gas). The resulting functional has been applied to bulk phases ranging from the nematic phase for spherocylinders [12] to the crystal for (rounded) parallel hard cubes [14], as well as the isotropic–nematic interface for spherocylinders [15] and inhomogeneous fluids of dumbbells [16] and polyhedra [17]. In addition, DFT functionals for particular shapes [18, 19] and fixed orientations [20, 21] can often be derived more elegantly and using fewer approximations than for the general case.

Recently, an FMT functional was derived from an approximated and resummed virial expansion [22]. This derivation justifies subsequent rescaling to obtain a better match to the next-lowest order virial diagram. A second advantage is that an accurate approximation for the virial expansion should be valid for all external potentials, not just for the homogeneous fluid and extremely confined systems. Finally and most importantly, the approximation performed on the virial expansion should be amendable to further improvements. Unfortunately, the derivation in Ref. [22] did not lead to the same functional as the one from the zero-dimensional limit [4], which is surprising as the approximated virial series is also exact [22] for the cavities where 0D-FMT is exact [4].

In this paper, we give an improved version of the derivation: First, it will be clear where the combinatorial prefactors in our approximated virial series come from. Secondly, we improve on the calculation of the intersection of three particles surfaces, which leads to consistency with 0D-FMT in three dimensions. Finally, we will consider explicitly all $d \leq 3$ spatial dimensions. The case $d < 3$ deserves to be considered explicitly, since many systems–colloidal suspensions in particular–exhibit interesting effects of reduced dimensionality [23]. Furthermore, an important test for the $d = 3$ functional is to evaluate it for the density profile of an extremely confined, quasi-d'-dimensional system with $d' < 3$ and compare to the results from the functional that is obtained directly by considering $d = d'$ explicitly [24].

This paper is organized as follows: We will first introduce some notation to allow for a reasonably compact form of our formula's in Sec. II. In Sec. III, we will for-

mally define the free energy in terms of a virial expansion. Subsequently, we will briefly describe the FMT functional [3, 11, 12] in Sec. IV. The general form of the functional motivates the approximation for the Mayer diagrams that we will use, which is the main result of Ref. [22]. We reiterate this approximation and show its relation to the Ree-Hoover resummation [25] of the Mayer diagrams in Sec. V. In Sec. VI, we will use a geometric approach to derive the functional without attempting to achieve full mathematical rigor. In Sec. VII, we will use the resulting geometrical expressions to resum our approximations for the Mayer diagrams to a closed form that turns out to be exactly equal to the 0D-FMT functional derived by Tarazona and Rosenfeld [4]. Our geometrical formulation of the functional allows us to calculate the direct correlation function using a formula from integral geometry, which we use to gauge the accuracy of the functional. Subsequently, we briefly reiterate the approximations and rescalings of the 0D-FMT functional that were performed to improve both the accuracy of FMT for certain common thermodynamic phases and the efficiency with which the functional can be evaluated in Refs. [4, 11, 26, 27]. Finally, we summarize our results, argue why the current functional is successful in the light of the virial expansion and discuss some improvements to the functional motivated by our derivation in Sec. VIII.

II. Notation

We will consider (in general) an M-components system of rigid particles in $1 \leq d \leq 3$ dimensions. In other words, a particle i is fully characterized by its species $s_i \in \{1, \ldots, M\}$, position $\mathbf{r}_i \in \mathbb{R}^d$ and orientation, specified by a rotation $\mathcal{R}_i \in \mathbb{SO}(d)$. We will denote this triplet of coordinates by $\mathbf{R}_i \equiv (\mathbf{r}_i, \mathcal{R}_i, s_i)$ and take $\mathbb{V}$ to mean the set of all accessible coordinates.

We also take the particles to have only-hard core interactions, that is the pair-wise interaction energy $\phi(\mathbf{R}_i, \mathbf{R}_j)$ between particles i and j is such that

$$e^{-\beta\phi(\mathbf{R}_i,\mathbf{R}_j)} = \begin{cases} 0 & \mathcal{B}(\mathbf{R}_i) \cap \mathcal{B}(\mathbf{R}_j) \neq \emptyset \\ 1 & \text{otherwise} \end{cases},$$

where $\mathcal{B}(\mathbf{R}_i)$ is the set of points in $\mathbb{R}^d$ inside a particle with coordinates $\mathbf{R}_i$. In principle, additional continuous coordinates could also be introduced and encoded in the tuple $\mathbf{R}$, for example, internal coordinates for molecules and size/shape for polydisperse systems. We will require that the sets $\mathcal{B}(\mathbf{R})$ are convex for all $\mathbf{R}$. We will also require that the boundaries $\partial\mathcal{B}(\mathbf{R})$ are twice differentiable, such that the principal curvatures $\kappa(\mathcal{B}, \mathbf{r})$ are well-defined for all points $\mathbf{r}$ on $\partial\mathcal{B}$ (or that the boundary can be obtained from a limiting process of twice differentiable surfaces as *e.g.* in Ref. [17]). We will often denote $\mathcal{B}(\mathbf{R}_i)$ as $\mathcal{B}_i$ and a property $\xi(\mathcal{B}_i, \mathbf{r})$ of the surface of a particle $\mathcal{B}_i$ at a point $\mathbf{r}$ by $\xi_i(\mathbf{r})$ or even ξ_i, if this does not cause confusion, *e.g.* the notation $\mathbf{n}_i$ for the normal vector is an abbreviation for $\mathbf{n}(\mathcal{B}_i, \mathbf{r})$.

For any function f on $\mathbb{V}$, we define

$$\int_{\mathbb{V}} \mathrm{d}\mathbf{R}\, f(\mathbf{R}) \equiv \sum_s \int_{\mathbb{R}^d} \mathrm{d}\mathbf{r} \int_{\mathbb{SO}(d)} \mathrm{d}\mathcal{R}\, f\big((\mathbf{r}, \mathcal{R}, s)\big);$$

n subsequent integrals over generalized coordinates will be denoted by $\int_{\mathbb{V}^n} \mathrm{d}\mathbf{R}^n$. Integration over an m-dimensional curved hypersurface A in $\mathbb{R}^d$ will be denoted by $\int_A d^m\mathbf{r}$ (with $m < d$). The unit $d-1$ sphere will be denoted by S_{d-1}, and its (hyper) surface area by $|S_{d-1}|$, while the spherical area of a subset $S \subset S_{d-1}$ will be denoted by $\sigma_{d-1}(S)$.

III. Density functional theory from a virial expansion

In density functional theory (DFT), the structure of the system is described by the density profile $\rho(\mathbf{R})$, which is defined such that the integral of ρ over a subset $A \subset \mathbb{V}$ is the average number of particles with generalized coordinates in A. Using Mayer's celebrated virial expansion, it can be shown that the grand-canonical free energy Ω of a system with an external potential $V_{\text{ext}}(\mathbf{R})$ can be written as a functional $\Omega[\rho_0]$ of the equilibrium density profile ρ_0. This grand potential functional is defined as

$$\Omega[\rho] \equiv \mathcal{F}[\rho] + \int_{\mathbb{V}} \mathrm{d}\mathbf{R}\, \rho(\mathbf{R})[V_{\text{ext}}(\mathbf{R}) - \mu_{\mathbf{R}}], \qquad (1)$$

where the chemical potential is denoted by $\mu_{\mathbf{R}}$, which only depends on the species component s of $\mathbf{R} = (\mathbf{r}, \mathcal{R}, s)$, see Sec. II. Often there will be $\mathbf{R} \in \mathbb{V}$ where $V_{\text{ext}}(\mathbf{R})$ is infinite; in this case, we set $V_{\text{ext}}(\mathbf{R})\rho(\mathbf{R}) = 0$ if $\rho(\mathbf{R}) = 0$. The intrinsic free energy $\mathcal{F}[\rho]$ consists of two parts,

$$\mathcal{F}[\rho] = \mathcal{F}_{\text{id}}[\rho] + \mathcal{F}_{\text{exc}}[\rho].$$

The first of these, the free energy functional for an ideal gas, $\mathcal{F}_{\text{id}}$, reads [2]

$$\mathcal{F}_{\text{id}}[\rho] = k_B T \int_{\mathbb{V}} \mathrm{d}\mathbf{R}\, \rho(\mathbf{R}) \log[\rho(\mathbf{R})\mathcal{V}] - \rho(\mathbf{R}),$$

where k_B denotes Boltzmann's constant, T the temperature and $\mathcal{V}$ is the thermal volume ($1/\mathcal{V}$ is defined as the integral over the momenta conjugate to $\mathbf{R}$ in the partition sum). Secondly, we define an explicit expression for the excess free energy $\mathcal{F}_{\text{exc}}[\rho]$ as an infinite series of Mayer diagrams [28, 29]:

$$-\beta\mathcal{F}_{\text{exc}}[\rho] = \sum_{n=2}^{\infty} \sum_{g \in \mathcal{M}[n]} g[\rho]$$

$$= \bullet\!\!-\!\!\bullet + \triangle + \square + \square + \boxtimes + \ldots, \qquad (2)$$

where $\beta = 1/k_B T$ and the set of n-node Mayer diagrams $\mathcal{M}[n]$ consists of all biconnected graphs with n nodes [30].

Each of these diagrams or graphs corresponds to a functional $g[\rho]$, which is constructed as follows: First, label all n circles or nodes of a graph g with indices 1 through n in some arbitrary way. Then define the set of index pairs $P(g) \subset \{1,\dots,n\}^2$, such that $(i,j) \in P(g)$ if and only if circle i and circle j are connected by a line in the graph g. With these definitions, the functional $g[\rho]$ reads

$$g[\rho] = \frac{1}{|\mathrm{Aut}(g)|} \int_{\mathbb{V}^n} \mathrm{d}\mathbf{R}^n \prod_{i=1}^{n} \rho(\mathbf{R}_i) \prod_{(i,j)\in P(g)} f_{\mathrm{M}}(\mathbf{R}_i,\mathbf{R}_j), \tag{3}$$

where $f_{\mathrm{M}}(\mathbf{R}_i,\mathbf{R}_j) = \exp[-\beta\phi(\mathbf{R}_i,\mathbf{R}_j)] - 1$ for particles interacting with a pairwise potential ϕ. For the hard particles of interest, $f_{\mathrm{M}}(\mathbf{R}_i,\mathbf{R}_j) = -1$ on overlap and $f_{\mathrm{M}}(\mathbf{R}_i,\mathbf{R}_j) = 0$ otherwise. Finally, the group of permutations of the nodes $1,\dots,n$ that map g to a diagram with the same connectivity is denoted by $\mathrm{Aut}(g)$ with order $|\mathrm{Aut}(g)|$ [the number of elements in the set of $\mathrm{Aut}(g)$]. We will also use the notation $|g|_L$ for the absolute value of the integral in Eqn. (3) without the factor $1/|\mathrm{Aut}(g)|$ (we use a subscript L, because $|g|_L$ is equal to the absolute value of the diagram g' formed by labeling the nodes of g, such that every circle is distinguishable from the others and $\mathrm{Aut}(g') = 1$).

It can be shown [2] that the equilibrium density profile ρ_0 of a system with the external potential $V_{\mathrm{ext}}(\mathbf{R})$ is equal to the density profile that minimizes the grand potential functional $\Omega[\rho]$ as defined in Ref. [2], provided that the set $\mathscr{M}$ of density profiles considered in the minimization contains ρ_0 and all ρ in $\mathscr{M}$ are v-representable. Here, a density profile ρ is called v-representable if an external potential v exists, such that ρ is equal to the equilibrium density profile of the system with external potential v and the same particle–particle interactions as the system of interest. For practical reasons, we restrict $\mathscr{M}$ to those ρ for which the virial expansions of $\mathcal{F}_{\mathrm{exc}}$ and $\frac{\delta}{\delta\rho(\mathbf{R})}\mathcal{F}_{\mathrm{exc}}$ converge (in practice, one often uses $\frac{\delta\Omega}{\delta\rho(\mathbf{R})} = 0$ to perform the minimization). This has the advantage that all ρ in $\mathscr{M}$ are v-representable; in fact, the external potential v which represents ρ is given by $v(\mathbf{R}) = \mu_{\mathbf{R}} - \frac{\delta\mathcal{F}}{\delta\rho(\mathbf{R})}$, which is obtained from $\frac{\delta\Omega}{\delta\rho} = 0$ by rearranging. Unfortunately, it cannot be guaranteed that the equilibrium density profile ρ is in $\mathscr{M}$, as convergence of the virial expansion is difficult to ascertain. However, the series in the approximation to $\mathcal{F}_{\mathrm{exc}}$ we will derive below always converges for the equilibrium density profile. In fact, the series converges for some density profiles that should not be in $\mathscr{M}$; for example, the functional predicts a finite free energy for the one-component homogeneous fluid for any packing fraction $\eta \le 1$, even if η is larger than the packing fraction in the close packed limit, $\eta_{\mathrm{cp}} \le 1$, where the packing fraction is defined as $\eta = Nv_p/V$ with the number of particles $N = \int_{\mathbb{V}} \mathrm{d}\mathbf{R}\,\rho(\mathbf{R})$, the volume of a particle v_p and the system volume V. Of course, such a branch of (local) minima of the grand potential can be easily dismissed as unphysical as it extends to $\eta \ge \eta_{\mathrm{cp}}$.

IV. Fundamental measure theory

In fundamental measure theory, the excess free energy is written as a functional of the following form

$$\mathcal{F}_{\mathrm{exc}} = \int_{\mathbb{R}^d} \mathrm{d}\mathbf{r}\,\Phi\big(\{n_A[\rho](\mathbf{r})\}\big), \tag{4}$$

where $\{n_A[\rho](\mathbf{r})\}$ is a set of weighted densities

$$n_A[\rho](\mathbf{r}) \equiv \int_{\mathbb{V}} \mathrm{d}\mathbf{R}\, w_A(\mathbf{R},\mathbf{r})\rho(\mathbf{R}) \tag{5}$$

(in the remainder we will drop the argument $[\rho]$ of n_A). These weight functions where originally derived from the low-density limit [3] for spheres in three dimensions, but subsequent generalizations all have this form. For $d = 3$, the super-index A takes values in $\{0,1,\dots,3\} \cup \{(\alpha,\tau,c)\,|\,\alpha \in \{1,2\},\ \tau \in \mathbb{N},\ c \in \{1,\dots,d\}^\tau\}$ where $\int_{\mathbb{R}^d}\mathrm{d}\mathbf{r}\, w_A(\mathbf{R},\mathbf{r})$ has dimension [length]$^\alpha$, τ denotes the tensor rank, and the index c denotes the tensor component. The weight functions $w_A(\mathbf{R},\mathbf{r})$ are distributions rather than functions. The first, w_d, is defined by

$$\int_{\mathbb{R}^d} \mathrm{d}\mathbf{r}\, f(\mathbf{r}) w_d(\mathbf{R},\mathbf{r}) \equiv \int_{\mathcal{B}(\mathbf{R})} \mathrm{d}\mathbf{r}\, f(\mathbf{r}), \tag{6}$$

for any function $f : \mathbb{R}^d \to \mathbb{R}$, that is, w_d simply restricts the integral to the interior of the particle. There is also a weight function that restricts the integral to the surface of the particles, namely, w_{d-1}.

$$\int_{\mathbb{R}^d} \mathrm{d}\mathbf{r}\, f(\mathbf{r}) w_{d-1}(\mathbf{R},\mathbf{r}) \equiv \int_{\partial\mathcal{B}(\mathbf{R})} \mathrm{d}^{d-1}\mathbf{r}\, f(\mathbf{r}) \tag{7}$$

Similarly, w_0 is defined by

$$\int_{\mathbb{R}^d} \mathrm{d}\mathbf{r}\, f(\mathbf{r}) w_0(\mathbf{R},\mathbf{r}) \equiv \int_{\partial\mathcal{B}(\mathbf{R})} \frac{K(\mathbf{r})}{|S_{d-1}|} \mathrm{d}^{d-1}\mathbf{r}\, f(\mathbf{r}), \tag{8}$$

where $K(\mathbf{r})$ is the Gaussian curvature of the surface at $\mathbf{r}$ and $|S_{d-1}|$ the spherical measure of the unit $d-1$ sphere. Finally, for $A \neq d, d-1, 0$, we only give the general form of the weight functions

$$\int_{\mathbb{R}^d} \mathrm{d}\mathbf{r}\, f(\mathbf{r}) w_A(\mathbf{R},\mathbf{r}) \equiv \int_{\partial\mathcal{B}(\mathbf{R})} \mathrm{d}^{d-1}\mathbf{r}\, \bar{w}_A(\mathbf{R},\mathbf{r}) f(\mathbf{r})$$

where $\bar{w}_A(\mathbf{R},\mathbf{r})$ contain local properties of the surface at $\mathbf{r}$ [11]. Clearly, the $w_A(\mathbf{R},\mathbf{r})$ for all A are invariant under simultaneous translation of the particle coordinates $\mathbf{R}$ and the position $\mathbf{r}$.

Taylor expanding the fundamental measure free energy density $\Phi(\{n_\alpha\})$ around $(n_0, n_1, \cdots) = (0, 0, \cdots)$ yields

$$\sum_{n=0}^{\infty} \frac{1}{n!} \sum_{A_1,\dots,A_n} \left.\frac{\partial^n \Phi}{\partial n_{A_1}\cdots\partial n_{A_n}}\right|_{n_A=0} \prod_{i=1}^{n} n_{A_i}.$$

Inserting this expression into the free energy (4), we see that the free energy can be written as

$$\mathcal{F}_{\rm exc} = \sum_{n=0}^{\infty} \int_{\mathbb{V}^n} \mathrm{d}\mathbf{R}^n \prod_{i=1}^{n} \rho(\mathbf{R}_i) \mathcal{K}_n(\mathbf{R}^n), \quad \text{where} \quad (9)$$

$$\mathcal{K}_n(\mathbf{R}^n) = \frac{1}{n!} \sum_{A_1,\ldots,A_n} \left. \frac{\partial^n \Phi}{\partial n_{A_1} \cdots \partial n_{A_n}} \right|_{n_A=0} \times \int_{\mathbb{R}^d} \mathrm{d}\mathbf{r} \prod_{i=1}^{n} w_{A_i}(\mathbf{R}_i, \mathbf{r}), \quad (10)$$

which is only nonzero if there is at least one $\mathbf{r}$ that is inside each particle $\mathcal{B}_i$, as a result of the range of the weight functions w_A. In other words, if we interpret (9) as a virial expansion, then in each n-particle diagram only configurations $\mathbf{R}^n$ with $\bigcap_{i=1}^n \mathcal{B}(\mathbf{R}_i) \neq \emptyset$ are included.

V. Stacks and Ree-Hoover diagrams

As we have just shown in Sec. IV, only n-particle configurations $\mathbf{R}^n$ with $\bigcap_{i=1}^n \mathcal{B}(\mathbf{R}_i) \neq \emptyset$ have to be taken into account in the n-th order virial term in order to obtain a functional of the FMT-form (4). For this reason, it was suggested in Ref. [22] to approximate a specific Mayer diagram by restricting the integral to configurations with a non-empty 'particle stack', where the 'stack', introduced in Ref. [22], is defined as

$$\mathrm{St}_n(\mathbf{R}^n) \equiv \bigcap_{i=1}^{n} \mathcal{B}(\mathbf{R}_i).$$

In Ref. [22], only the fully connected Mayer-diagram (the diagram where each node is connected to all other nodes by Mayer-bonds) was included in the virial expansion; all other diagrams were neglected. Subsequently, a somewhat involved argument was used to obtain a free energy that is of the FMT form. Here, we retain all Mayer diagrams and apply the same approximation as in Ref. [22] to every diagram, which allows a more straightforward route using only the virial expansion.

The approximation to only include $\mathbf{R}^n$ with non-empty $\mathrm{St}_n(\mathbf{R}^n)$ in a Mayer diagram greatly simplifies the corresponding integrals, because it implies that each particle overlaps with each other particle or, equivalently, $f_{\rm M}(\mathbf{R}_i, \mathbf{R}_j) = -1$ for $1 \leq i \neq j \leq n$. As a result, the product of the Mayer bonds in each Mayer diagram g with n nodes, *cf.* Eqn. (3), becomes

$$\prod_{(i,j)\in P(g)} f_{\rm M}(\mathbf{R}_i, \mathbf{R}_j) \to (-1)^{|P(g)|} \chi'(\mathbf{R}^n) \quad (11)$$

where $$\chi'(\mathbf{R}^n) = \begin{cases} 1 & \text{if } \mathrm{St}_n(\mathbf{R}^n) \text{is non-empty} \\ 0 & \text{otherwise} \end{cases}$$

and $|P(g)|$ denotes the number of elements of $P(g)$, or, equivalently, the number of lines in g. In order to simplify this expression further in Sec. VI, we have to introduce a notion from geometry, namely the Euler characteristic. The Euler characteristic $\chi(S)$ of a subset S of $\mathbb{R}^d$ is equal to one when S is a convex set and zero when S is empty. Therefore, $\chi'(\mathbf{R}^n)$ is equal to $\chi[\bigcap_{i=1}^n \mathcal{B}(\mathbf{R}_i)]$ as we have restricted ourselves to convex bodies, see Sec. II, and the intersection of any number of convex sets is either convex or empty. As $\chi(S)$ is a topological invariant, $\chi(S)$ is also equal to one if S is a smooth deformation of a convex set, such as the set that we will encounter in Sec. VI A 5. In other cases, $\chi(S)$ can have any integer value (positive, negative or zero). Therefore, $\chi'(\mathbf{R}^n) = \chi[\bigcap_{i=1}^n \mathcal{B}(\mathbf{R}_i)]$ does not hold in general for non-convex particles whose intersections can be topologically nontrivial.

Collecting all approximated Mayer diagrams with the same number of nodes, the approximation for the excess free energy from the virial expansion (2) can be written as

$$\sum_{n=2}^{\infty} c_n \int_{\mathbb{V}^n} \mathrm{d}\mathbf{R}^n \, \chi\big[\bigcap_{i=1}^n \mathcal{B}(\mathbf{R}_i)\big] \prod_{i=1}^n \rho(\mathbf{R}_i), \quad (12)$$

where we introduced the combinatorial factor c_n,

$$c_n \equiv - \sum_{g\in\mathcal{M}[n]} \frac{1}{|\mathrm{Aut}(g)|} (-1)^{|P(g)|}. \quad (13)$$

It remains to obtain a closed form for c_n as a function of n. The latter problem has already been solved by Ree and Hoover in the context of their resummation of the Mayer diagrams to obtain an efficient algorithm for the virial expansion for homogeneous fluids of hard spheres [25, 31]. They introduced a new type of diagram, which we will call a Ree-Hoover diagram, which contains Ree-Hoover bonds $e_{\rm RH} \equiv 1 - f_{\rm M}$ in addition to the Mayer bonds f_M. The systematic resummation of the Mayer diagrams into Ree-Hoover diagrams is obtained in the following way [25]: First, the integrand of each Mayer diagram g is multiplied by a factor $1 = e_{\rm RH}(\mathbf{R}_i, \mathbf{R}_j) - f_{\rm M}(\mathbf{R}_i, \mathbf{R}_j)$ for every pair of nodes (i, j) that is not connected by a line in g. Subsequently, one expands the resulting expression in products of $e_{\rm RH}(\mathbf{R}_i, \mathbf{R}_j)$ and $f_M(\mathbf{R}_i, \mathbf{R}_j)$ functions, and finally, the diagrams g that have the same $|g|_L$ are collected into one diagram, which we call a Ree-Hoover diagram. It can be easily seen that each Ree-Hoover diagram $g_{\rm RH}$ contains the contributions of all configurations for which a given pair of particles i and j is either required to overlap, if i and j are connected by an $f_{\rm M}$-bond in $g_{\rm RH}$, or i and j are not allowed to overlap, if i and j are connected by a $e_{\rm RH}$-bond in $g_{\rm RH}$. Ree and Hoover abbreviated the diagrams by leaving out the $f_{\rm M}-$bonds and denoted the n-particle diagram without $e_{\rm RH}$-bonds by the symbol for the empty set $(\emptyset)_n$.

The Ree-Hoover resummation reduces the amount of cancellation between different diagrams in the virial series: The configurations in a class in which P is the set of overlapping pairs contribute to all Mayer diagrams g for which at least each pair of nodes in P is connected by a line, that is, all g for which $P \subset P(g)$. Therefore, for

many classes with overlapping particles in P, the negative contributions to diagrams with an odd number of bonds partially cancel the positive contributions to the Mayer diagrams with an even number of bonds. In particular, each n-particle configuration that contributes to the $(\emptyset)_n$ diagram contributes to all Mayer diagrams, but with different prefactors (with oscillating signs), such that

$$(\emptyset)_n = \sum_{g\in\mathcal{M}[n]} \frac{1}{|\mathrm{Aut}(g)|}(-1)^{|P(g)|}|s_n|_L,$$

where s_n is the fully connected *Mayer* diagram. We see that the prefactor is equal to $-c_n$, where c_n is defined in Eqn. (13). In other words, we would have obtained the same functional if we had started our derivation with the Ree-Hoover resummation of the Mayer diagrams, only retained the $(\emptyset)_n$ diagrams and, finally, neglected those configurations $\mathbf{R}^n$ in the integrals of $(\emptyset)_n$ where $\mathrm{St}_n(\mathbf{R}^n) = \emptyset$. Following Tarazona and Rosenfeld [4], we will use the term 'lost cases' for the configurations neglected in the latter approximation.

Combinatorial techniques for the Mayer diagrams [32], which are beyond the scope of this work, have been used to find a closed form for the prefactor c_n as a function of n. In our case, it is found [25] that the prefactor c_n is

$$c_n = 1/[n(n-1)]. \tag{14}$$

As an aside, we note that the prefactor of Ree-Hoover diagrams with a small number of e_{RH}-bonds can be conveniently calculated using techniques from Refs. [33, 34] if the prefactor of the smallest such diagrams is known.

VI. Geometry of a stack

We wish to find an expression for $\chi(\mathrm{St}_n)$ (where $\mathrm{St}_n = \bigcap_{i=1}^n \mathcal{B}(\mathbf{R}_i)$ as before) that allows summation of the free energy (12) to a closed form. In order to do this we will require some concepts from integral geometry, which we will introduce along the way. More information and more definitions for more general (non-smooth) convex bodies can be found in *e.g.* Refs. [35] and [36].

As noted by Gauss for three-dimensions, there exists a natural map, the Gauss map, from the surface of a smooth d-dimensional body to the d-dimensional unit sphere S_{d-1}, where a point $\mathbf{p}$ on the surface is mapped to the outer normal of the surface at $\mathbf{p}$. We will use a slight extension for non-smooth particles, where a point $\mathbf{p}$ on the surface $\partial\mathcal{B}$ of a body $\mathcal{B}$ is mapped to the 'normal cone', defined as

$$N^+(\mathcal{B},\mathbf{p}) = \{\mathbf{n}\in S_{d-1} | \mathbf{n}\cdot(\mathbf{b}-\mathbf{p}) \le 0 \quad \forall \mathbf{b}\in\mathcal{B}\}.$$

If $\partial\mathcal{B}$ is locally smooth at $\mathbf{p}$, $N^+(\mathcal{B},\mathbf{p})$ is a set with one element, the unique normal at $\mathbf{p}$. Note, that the definition of the normal cone $N^+(\mathcal{B},\mathbf{p})$ is only useful for convex particles: $N^+(\mathcal{B}_{nc},\mathbf{p}) = \emptyset$ for a point $\mathbf{p}$ on the concave part of the surface of a non-convex body $\mathcal{B}_{nc}$. We can straightforwardly extend this definition to (Borel) subsets A of $\mathbb{R}^d$ to obtain the normal cone of A,

$$N^+(\mathcal{B},A) = \bigcup_{\mathbf{p}\in A\cap\partial\mathcal{B}} N^+(\mathcal{B},\mathbf{p}). \tag{15}$$

The spherical measure $\sigma_{d-1}(\cdot)$ of the normal cone relative to the total measure of the $(d-1)$ sphere $|S_{d-1}|$ will play a central role in our derivation, so we will use a separate symbol $\gamma(\mathcal{B},\cdot)$ for the corresponding measure,

$$\gamma(\mathcal{B},A) \equiv \frac{\sigma_{d-1}\big(N^+(\mathcal{B},A)\big)}{|S_{d-1}|}.$$

for any (Borel) subset $A\subset\mathbb{R}^d$. Applying this measure to the stack, we can write

$$\chi\big(\textstyle\bigcap_{i=1}^n \mathcal{B}_i\big) = \gamma(\mathrm{St}_n,\mathbb{R}^d) = \gamma(\mathrm{St}_n,\partial\mathrm{St}_n). \tag{16}$$

Here and in the remainder of this section (Sec. VI), we write $\mathcal{B}_i$ instead of $\mathcal{B}(\mathbf{R}_i)$. Of course, if $\mathrm{St}_n = \emptyset$, $N^+(\mathrm{St}_n,\mathbf{p}) = \emptyset$ and $\gamma(\mathrm{St}_n,\mathbf{p}) = 0$ for all $\mathbf{p}\in\mathbb{R}^d$, while $N^+(\mathrm{St}_n,\mathbb{R}^d)$ is the full unit sphere if St_n is non-empty, such that $\gamma(\mathrm{St}_n,\mathbb{R}^d) = 1$, which proves Eqn. (16) for a stack of *convex* particles.

In our case, this is useful because of the following decomposition:

$$\begin{aligned}
&N^+(\mathrm{St}_n,\partial\mathrm{St}_n)\\
&= \bigcup_{i=1}^n N^+\big(\mathrm{St}_n,\partial\mathcal{B}_i\cap\mathrm{St}^{\cup}_{n\setminus i}\big)\\
&\cup \bigcup_{\substack{i,j=1\\ i<j}}^n N^+\big(\mathrm{St}_n,\partial\mathcal{B}_i\cap\partial\mathcal{B}_j\cap\mathrm{St}^{\cup}_{n\setminus i,j}\big)\\
&\cup \ldots\\
&\cup \bigcup_{\substack{i_1,\ldots,i_m=1\\ i_1<\ldots<i_m}}^n N^+\big(\mathrm{St}_n,\partial\mathcal{B}_{i_1}\cap\ldots\cap\partial\mathcal{B}_{i_m}\cap\mathrm{St}^{\cup}_{n\setminus i_1,\ldots,i_m}\big)
\end{aligned} \tag{17}$$

where we have defined the *open* subset of $\mathbb{R}^d$,

$$\mathrm{St}^{\cup}_{n\setminus i_1,\ldots,i_m} \equiv \bigcap_{\substack{\nu=1\\ \nu\neq i_1,\ldots,\nu\neq i_n}}^n \mathrm{int}(\mathcal{B}_\nu).$$

Here, $\mathrm{int}(\mathcal{B})$ is the interior of the body $\mathcal{B}$ *i.e.* $\mathrm{int}(\mathcal{B}) = \mathcal{B}\setminus\partial\mathcal{B}$. An example of the decomposition (17) in $d=2$ dimensions is shown in Fig. 1.

In the remainder of this section, we will exclude some pathological n-particle configurations with a vanishing contribution to the free energy, namely those for which one or more surfaces $\partial\mathcal{B}_i$ are tangent to either another surface $\partial\mathcal{B}_j$ or the intersection between two or more of the other surfaces or for which the intersection between d particles in d dimensions lies on one of the surfaces. With this restriction, the intersection between k surfaces is always a $(d-k)$-dimensional subset of $\mathcal{R}^d$. As a result,

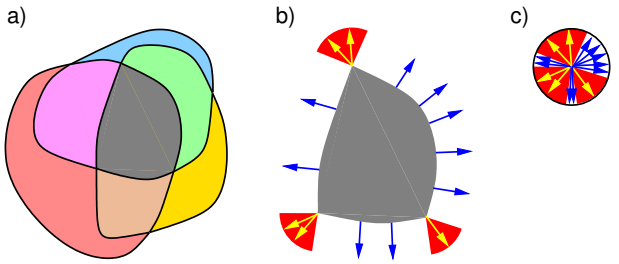


FIG. 1. (a) Example of a 'stack' in two dimensions: The dark area denotes the 'stack' of three arbitrary convex bodies, defined as the intersection between the bodies. The main approximation necessary to derive FMT is to restrict the multi-dimensional integrals in the Mayer diagrams to include only those configurations as shown here, that is, where the intersection between all bodies is non-empty. (b) and (c) The union of all normal vectors of the surface of a convex body (b) is just the $(d-1)$-dimensional unit hyper-sphere (c), (a circle with unit radius for $d=2$). The set of vectors normal to a point $\mathbf{p}$ on the surface of a stack, $N^+(\mathbf{p})$, can either contain a single normal vector for a point $\mathbf{p}$ on one of the surfaces of the particles that constitute the stack (examples are the dark arrows) or a $(k-1)$-dimensional set of normal vectors for $\mathbf{p}$ on the intersection between k surfaces (*e.g.* the sectors containing the light arrows for $k=2$).

the number of elements in the union (17), m, is at most $\min\{n,d\}$ in d dimensions [37]. Note, that the surface of the stack is non-smooth near all points $\mathbf{p}$ on the intersections of k surfaces ∂B_i (for $k\geq 2$), and that $N^+(\mathrm{St}_n,\mathbf{p})$ is a $(k-1)$-dimensional set for such points $\mathbf{p}$. For *convex* particles, we know that every unit vector is an outer normal vector to the surface in exactly one point, which implies that the sets in the union (17) are pairwise disjoint (more precisely $\sigma_{d-1}(A\cap B)=0$ for any two sets A, B in the union (17) with $A\neq B$). Therefore,

$$\gamma(\mathrm{St}_n,\partial\mathrm{St}_n) = \sum_{k=1}^{m}\sum_{\substack{i_1,\ldots,i_k=1\\ i_1<\ldots<i_k}}^{n}\gamma\big(\mathrm{St}_n,\partial\mathcal{B}_{i_1}\cap\ldots\cap\partial\mathcal{B}_{i_k}\cap\mathrm{St}^{\cup}_{n\setminus i_1,\ldots,i_k}\big),$$

which is also obvious from the fact that $\gamma(B,\cdot)$ is additive [36]. The decomposition of γ is a special case of the decomposition of local Minkowski functionals [38]. Consider a $d-k$ dimensional intersection Σ_{d-k} of k surfaces of some convex bodies $\{\mathcal{B}_j\}_{j=1}^k$ for $2\leq k\leq d$. Using the Lebesgue integral with $\gamma(B,\cdot)$ as the integration measure, we can now formally define a generalized weight function $w^{[k]}(\mathcal{B}_1,\ldots,\mathcal{B}_k,\mathbf{r})$ by

$$\int_{\mathbb{R}^d}\mathrm{d}\mathbf{r}\, f(\mathbf{r})w^{[k]}(\mathcal{B}_1,\ldots,\mathcal{B}_k;\mathbf{r}) \equiv \frac{1}{k!}\int_{\Sigma_{d-k}\subset\mathbb{R}^d}\gamma(\mathcal{B}_1\cap\cdots\cap\mathcal{B}_k,\mathrm{d}\mathbf{p})\, f(\mathbf{p}) \quad (18)$$

for any piecewise continuous function $f(\mathbf{r})$ on $\mathbb{R}^d$. We have absorbed a factor $1/k!$ into the generalized weight function that would have otherwise appeared explicitly in the excess free energy functional $\mathcal{F}_{\mathrm{exc}}$ in Sec. VII.

With this definition (18), we can write the normalized normal cone area of the stack as

$$\gamma\big(\mathrm{St}_n,\partial\mathrm{St}_n\big) = \int_{\mathbb{R}^d}\mathrm{d}\mathbf{r}\sum_{k=1}^{m}\sum_{\substack{i_1,\ldots,i_k=1\\ i_1\neq\ldots\neq i_k}}^{n} w^{[k]}\big(\mathcal{B}_{i_1},\cdots,\mathcal{B}_{i_k};\mathbf{r}\big)\prod_{\substack{j=1\\ j\notin\{i_1,\cdots,i_k\}}}^{n} w_d(\mathcal{B}_j,\mathbf{r}), \quad (19)$$

with the volume weight function w_d from Eqn. (6). This expression suffices to resum the approximated Mayer diagrams in a closed form to obtain a functional. However, the expressions for the k-weight functions (18) for $k\geq 2$ are not very useful for explicit calculations and they are difficult to compare to the FMT weight functions. Therefore, we specialize to cases where we can give explicit expressions in Sect. VI A.

A. Special cases

In this section, we will restrict ourselves to the relevant cases for the spatial dimensions $1\leq d\leq 3$, namely $k=d=1$; $k=d$ for $d=2,3$; $k=1$ for general $d>1$ and, finally, $k=2$ for $d=3$. For these cases, we will obtain explicit expressions for the resulting weight functions, which are summarized in Table I. The general case will be discussed elsewhere [39].

1. *One dimension*

For $d=1$, every $\mathcal{B}_i=[a_i,b_i]$ for some real numbers a_i and b_i and we have $m=1$ since the boundaries of the particles cannot intersect. The stack for $d=1$ is illustrated in Fig. 2. It is non-empty if $\min_i b_i>\max_i a_i$, in which case the normal cone of the stack [as defined in Eqn. (15)] consist of the normal vectors $+1$ at $\min_i b_i$ and -1 at $\max_i a_i$. (The 0-dimensional unit sphere consist of the two points ±1 and $|S_0|=2$.) The normal cone area for δB_i in $d=1$ dimensions has the form (19) with

$$w^{[1]}(\mathcal{B}_i;x)\equiv\sum_{p\in\{a_i,b_i\}}\tfrac{1}{2}\delta(x-p).$$

2. *Intersection between d particles (k = d)*

We will first consider $k=d$ intersecting surfaces for general d. The set $\Sigma_{d-k}=\Sigma_0$ is then a set of discrete points at which the boundaries intersect. Therefore, we

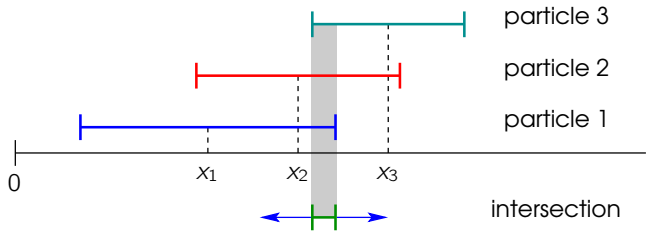


FIG. 2. In one dimension, 'particles' are line intervals and only two normals are possible, +1 and −1, as shown by the arrows. The 'stack' of the three particles shown is the line interval labeled 'intersection'.

can immediately write down the $w^{[k]}$,

$$w^{[d]}(\mathcal{B}_{i_1},\dots,\mathcal{B}_{i_k};\mathbf{r}) \equiv \sum_{\mathbf{p}\in\Sigma_0} \frac{\sigma_{d-1}\big(N^+(\mathrm{St}_n,\mathbf{p})\big)}{|S_{d-1}|k!}\delta(\mathbf{r}-\mathbf{p}), \tag{20}$$

where explicit expressions for $\sigma_{d-1}\big(N^+(\mathrm{St}_n,\mathbf{p})\big)$ are given below for $d=2,3$. Note, that $w^{[1]}$ for $d=1$ is consistent with the expression obtained in Sec. VI A 1.

3. *No intersection ($k=1$)*

In order to discuss $k=1$ for $d>1$ [the case $k=d=1$ is already covered by Eqn. (20)], we will use the equality ([36], page 608 in [35]) of γ and Φ_0, one of the curvature measures [40], which for a smooth body and some (Borel) subset $A\subset\mathbb{R}^d$ reads

$$\Phi_0(\mathcal{B},A) = \int_{\partial B\cap A} \mathrm{d}^{d-1}\mathbf{r}\,\frac{K(\mathbf{r})}{|S_{d-1}|} = \gamma(\mathcal{B},A) \tag{21}$$

where $K(\mathbf{r})$ is the Gaussian curvature at $\mathbf{r}$: $K\equiv\prod_{j=1}^{d-1}\kappa^j$, where the principal curvature in direction $\mathbf{v}^j$ is denoted by κ^j for $1\le j\le d-1$. The equality between the integrated Gaussian curvature $\Phi_0(\mathcal{B},A)$ and the normal cone area $\gamma(\mathcal{B},A)$ (which, in its original version in $d=3$ dimensions is due to Gauss) is illustrated in Fig. 3. Using this equality, we can define $w^{[1]}$ as

$$w^{[1]}(\mathcal{B}_i,\mathbf{r}) = \frac{K_i(\mathbf{r})}{|S_{d-1}|}w_{d-1}(\mathcal{B}_i,\mathbf{r}), \tag{22}$$

which is equal to the FMT weight function w_0, see Eqn. (8). Here, we used the weight function w_{d-1} as defined in Eqn. (7).

4. *Two dimensions*

For the case $k=d=2$, the normal cone of the intersection point is just the arc spanned by the normal vectors $\mathbf{n}_1$ and $\mathbf{n}_2$ of the two intersecting surfaces and the arc length reads

$$\sigma_1\big(N^+(\mathrm{St}_n,\mathbf{p})\big) = \arccos(\mathbf{n}_1\cdot\mathbf{n}_2). \tag{23}$$

Using this arc length in Eqn. (20) for $d=2$, the weight function $w^{[2]}$ is defined. For the remaining case, $k=1$ in $d=2$ dimensions, we can use the expression (22) for $w_0^{[1]}$ given above.

5. *Three dimensions: the Gauss-Bonnet theorem*

The intersection of three bodies in three dimensions with the three different types of contributions ($k=1,2,3$) to the normal cone is shown in Fig. 4.

First, the weight function $w^{[1]}$ as defined in (22) can be used. Secondly, the normal cone for $d=k=3$ is a spherical triangle spanned by the normal vectors $\mathbf{n}_1$, $\mathbf{n}_2$ and $\mathbf{n}_3$ of the three intersection surfaces. Its area reads

$$\sigma_2\big(N^+(\mathrm{St}_n,\mathbf{p})\big) = \alpha_{123}+\alpha_{231}+\alpha_{312}-\pi \quad \text{for } d=3,$$

which can be inserted in Eqn. (20) for $d=3$ to define the weight function $w^{[3]}$. Here, α_{ijk} denotes the dihedral angle, as depicted in Fig. 4(a), which reads

$$\alpha_{ijk} = \arccos(\mathcal{N}[\mathbf{n}_i\times\mathbf{n}_j]\cdot\mathcal{N}[\mathbf{n}_k\times\mathbf{n}_j]),$$

where $\mathcal{N}[\mathbf{v}]$ for $\mathbf{v}\in\mathbb{R}^d$ denotes the normalized vector $\mathbf{v}/|\mathbf{v}|$ and the cross product (in $d=3$ only) is denoted by $\times$.

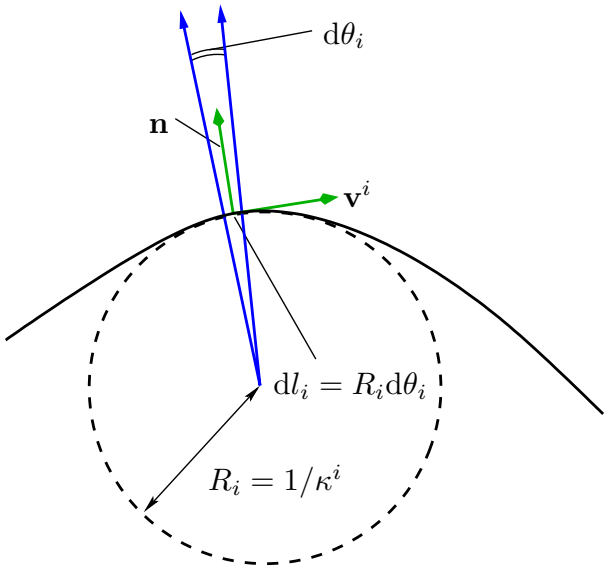


FIG. 3. Illustration of the equality of γ and Φ_0, see Eqn. (21). The radius of curvature $R_i=1/\kappa^i$ in principal direction $\mathbf{v}^i$ at some point $\mathbf{p}$ is illustrated by the dashed circle. The intersection between the surface $\partial\mathcal{B}$ of a particle $\mathcal{B}$ and the plane spanned by $\mathbf{v}^i$ and the normal vector $\mathbf{n}$ at $\mathbf{p}$ is denoted by the black curve. The extension in direction $\mathbf{v}_i$ of the normal cone to an infinitesimally small patch $\mathrm{d}A$ of the surface near $\mathbf{p}$ is denoted by the angle $\mathrm{d}\theta_i\simeq\mathrm{d}l_i/R_i=\kappa^i\mathrm{d}l_i$, where $\mathrm{d}l_i$ is the extension of the patch in direction $\mathbf{v}^i$. Now, the spherical area of the normal cone to $\mathrm{d}A$ can be seen to be equal to the Gaussian curvature integrated over $\mathrm{d}A$: $|S_{d-1}|\gamma(\mathcal{B},\mathrm{d}A)\simeq\prod_i\mathrm{d}\theta_i\simeq\prod_i\kappa_i\mathrm{d}l_i\simeq\Phi_0(\mathcal{B},\mathrm{d}A)|S_{d-1}|$.

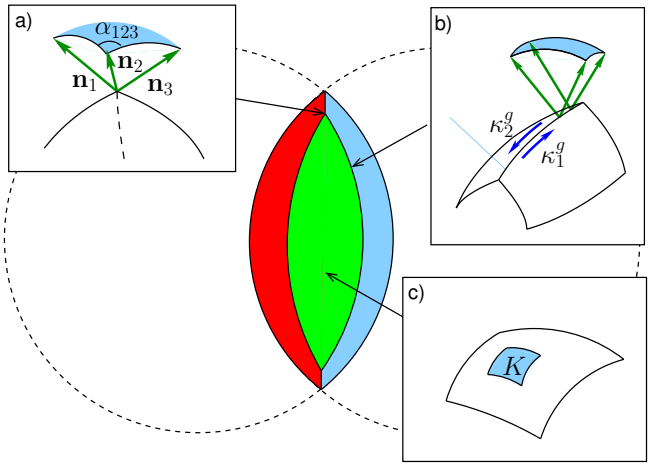


FIG. 4. The intersection between three particles (spheres in this case) in three dimensions (the surfaces of the three spheres have different colors for clarity). For $d = 3$, there are three contributions that are distinguished by the number of intersecting surfaces k as shown in the three panels: (a) $k = 3$ (b) $k = 2$ and (c) $k = 1$. For $k = 3$ surfaces that intersect at a point $\mathbf{p}$, the normal cone $N^+(\mathbf{p})$ is a spherical triangle spanned by the normals of the intersecting surfaces at $\mathbf{p}$ depicted by the arrows in (a). For $k = 2$ and $k = 1$, the contribution of a small section of the intersection (b) or the surfaces itself (c) is indicated by the filled area. In (b), we also indicated the geodesic curvatures κ_1^g and κ_2^g of the paths indicated by arrows with the corresponding labels.

Finally, the normal cones for $k = 2$ in three dimensions, or $1 < k < d$ for general $d \geq 3$, contain continuous $(d-k)$-dimensional sets of points that contribute to the total normal cone, which requires a different way of calculating the total normal cone area of the stack. One option would be to use Chern's direct approach [41]. Instead, we will perform a less involved calculation using the Gauss-Bonnet theorem, which reads (in three dimensions),

$$\int_S K \mathrm{d}A + \sum_k \int_{\partial S_k} \kappa_g \mathrm{d}l + \sum_n \angle_n = 2\pi\chi(S), \qquad (24)$$

where S is a compact twice differentiable two-dimensional surface bounded by an oriented curve ∂S consisting of M smooth sections ∂S_k, while the curve turns by $\angle_n$ at the intersection between sections ∂S_{n-1} and ∂S_n (and $\partial S_0 \equiv \partial S_M$). Furthermore, K is the Gaussian curvature and κ_g is the geodesic curvature on the smooth sections of ∂S. Finally, $\chi(S)$ is the Euler characteristic of the surface.

The Gauss-Bonnet theorem cannot be directly applied to the stack because it is not smooth (the Gaussian curvature is not well-defined on the intersection between two or three surfaces), so we will consider the 'tube' or the surface parallel to a subset A of the surface of the stack:

$$t_\epsilon(A) = \bigcup_{\mathbf{p}\in A} \epsilon N^+(\mathrm{St}_n, \mathbf{p}) + \mathbf{p}$$

(where scaling a set by a constant and summing a set and a vector implies performing the operation to each element separately: $\mathbf{p} + \epsilon C := \epsilon C + \mathbf{p} := \{\mathbf{p} + \epsilon\mathbf{r} | \mathbf{r} \in C\}$ for any set $C \subset \mathbb{R}^d$). The parallel body is defined by

$$(\mathcal{B})_\epsilon = \{\mathbf{p} + \mathbf{r} : \mathbf{p} \in \mathcal{B}, \mathbf{r} \in \mathbb{R}^d, |\mathbf{r}| \leq \epsilon\}. \qquad (25)$$

Note that the normal cone of a subsection S of $\partial \mathrm{St}_n$ is the same as the normal cone of the surface parallel to S: $N^+\left(t_\epsilon S, (\mathrm{St}_n)_\epsilon\right) = N^+(S, \mathrm{St}_n)$; however, $t_\epsilon S$ is always a twice-differentiable $(d-1)$-dimensional hypersurface even if S is not. With these definitions, we can consider the remaining case: $k = 2$ intersecting surfaces in $d = 3$ dimensions. A very similar calculation was also used to decompose the Mayer bond into weight functions [11, 26].

We will consider a subsection δC of the curve $\Sigma_2 = \partial B_{i_1} \cap \partial B_{i_2}$ and consider the normal cone of $t_\epsilon \delta C$ [the latter is denoted by the light blue area in Fig. 4 b)]. The direct approach, integrating the Gaussian curvature K over $t_\epsilon \delta C$, has been followed in Refs. [13, 22] and will not be repeated here.

As a second approach [13], which connects to the deconvolution of the Mayer bond in Ref. [11], the Gauss-Bonnet theorem, Eqn. (24) can be applied for $S = t_\epsilon \delta C$. The boundary ∂S consists of the arcs

$$\partial S_1 = \{\mathbf{a} + \epsilon[\cos\phi \mathbf{e}_1(\mathbf{a}) + \sin\phi \mathbf{e}_2(\mathbf{a})] : |\phi| < \phi_{ij}(\mathbf{a})/2\},$$
$$\partial S_3 = \{\mathbf{b} + \epsilon[\cos\phi \mathbf{e}_1(\mathbf{b}) + \sin\phi \mathbf{e}_2(\mathbf{b})] : |\phi| < \phi_{ij}(\mathbf{b})/2\},$$

which have zero geodesic curvature, and the curves

$$\partial S_2 = \{\mathbf{r} + \epsilon \mathbf{n}_i(\mathbf{r}) | \mathbf{r} \in \delta C\} \quad \text{and}$$
$$\partial S_4 = \{\mathbf{r} + \epsilon \mathbf{n}_j(\mathbf{r}) | \mathbf{r} \in \delta C\},$$

whose geodesic curvatures reduce to those of δC on the two respective surfaces when $\epsilon \to 0$. Here, $\mathbf{a}$ and $\mathbf{b}$ are the end points of the curve δC; the angle ϕ_{ij} is defined as $\phi_{ij} \equiv \arccos(\mathbf{n}_i \cdot \mathbf{n}_i)$; $\mathbf{e}_1 = (\mathbf{n}_1 + \mathbf{n}_2)/\sqrt{2(1 + \mathbf{n}_1 \cdot \mathbf{n}_2)}$ and $\mathbf{e}_2 = (\mathbf{n}_1 - \mathbf{n}_2)/\sqrt{2(1 - \mathbf{n}_1 \cdot \mathbf{n}_2)}$. It can easily be seen that the angles $\angle_n$ between the curves ∂S_n and ∂S_{n+1} are equal to $\pi/2$ for all n. Applying the Gauss-Bonnet theorem to $S = t_\epsilon \delta C$, rearranging and inserting the above expressions for the geodesic curvatures and angles $\angle_n$, we obtain

$$\lim_{\epsilon\to 0} \int_S \mathrm{d}^2\mathbf{r}\, K(\mathbf{r}) =$$
$$\lim_{\epsilon\to 0} \left[2\pi - 4 \times \pi/2 - \int_{\partial S_2} \mathrm{d}^1\mathbf{r}\, \kappa_i^g(\mathbf{r}) - \int_{\partial S_4} \mathrm{d}^1\mathbf{r}\, \kappa_j^g(\mathbf{r})\right]$$
$$= \int_{\delta C} \mathrm{d}^1\mathbf{r}\, [\kappa_i^g(\mathbf{r}) + \kappa_j^g(\mathbf{r})].$$

Therefore, the generalized weight function for $k = 2$ and $d = 3$ is defined by

$$\int_{\mathbb{R}^d} \mathrm{d}\mathbf{r}\, f(\mathbf{r}) w^{[2]}(\mathcal{B}_i, \mathcal{B}_j, \mathbf{r}) = \int_{\partial\mathcal{B}_i \cap \partial\mathcal{B}_j} \mathrm{d}^1\mathbf{r}\, \frac{\kappa_i^g + \kappa_j^g}{8\pi} f(\mathbf{r})$$

d	k	$Q_d^{[k]}(\mathcal{B}_1,\dots,\mathcal{B}_k;\mathbf{r})$
1	1	$\frac{1}{2}$
2	1	$\frac{K_1}{2\pi}$
	2	$\sqrt{1-(\mathbf{n}_1\cdot\mathbf{n}_2)^2}\,\frac{\arccos(\mathbf{n}_1\cdot\mathbf{n}_2)}{4\pi}$
3	1	$\frac{K_1}{4\pi}$
	2	$\lvert\mathbf{n}_1\times\mathbf{n}_2\rvert\,\frac{\kappa_1^g+\kappa_2^g}{8\pi}$
	3	$\lvert\mathbf{n}_1\cdot(\mathbf{n}_2\times\mathbf{n}_3)\rvert\,\frac{\alpha_{123}+\alpha_{231}+\alpha_{312}-\pi}{24\pi}$

TABLE I. As shown in the text, all k-body weight functions, $w^{[k]}(\mathcal{B}_1,\dots,\mathcal{B}_k;\mathbf{r})$ have the form $Q_d^{[k]}(\mathcal{B}_1,\dots,\mathcal{B}_k;\mathbf{r})\prod_{i=1}^k w_{d-1}(\mathcal{B}_i,\mathbf{r})$ in d spatial dimensions with the factors $Q_d^{[k]}$ that are listed in this table. See text for the definitions of the symbols; K_1, $\mathbf{n}_i$, κ_i^g and α_{ijk} depend implicitly on the point $\mathbf{r}$ and the body/bodies with the corresponding index/indices. For comparison to Refs. [4, 11, 26, 27], we wrote $[\mathbf{n}_1]=1$ and $[\mathbf{n}_1,\mathbf{n}_2]=\sqrt{1-(\mathbf{n}_1\cdot\mathbf{n}_2)^2}$, which are valid for general d, as well as $[\mathbf{n}_1,\mathbf{n}_2]=|\mathbf{n}_1\times\mathbf{n}_2|$ and $[\mathbf{n}_1,\mathbf{n}_2,\mathbf{n}_3]=|\mathbf{n}_1\cdot(\mathbf{n}_2\times\mathbf{n}_2)|$ which are valid only for $d=3$.

This can be seen to be equal to the result from Ref. [22] using the explicit expression for the geodesic curvature from Refs. [11, 13],

$$\kappa_i^g+\kappa_j^g=\frac{\kappa_i^{II}(\mathbf{v}_i^I\cdot\mathbf{n}_j)^2+\kappa_i^I(\mathbf{v}_i^{II}\cdot\mathbf{n}_j)^2}{|\mathbf{n}_i\times\mathbf{n}_j|\,(1+\mathbf{n}_i\cdot\mathbf{n}_j)}+(i\leftrightarrow j).$$

where $(i\leftrightarrow j)$ means the preceding expression with i and j interchanged. This concludes the calculation of the k-body weight function in the form given in Eqn. (18) for the special cases $k=1,d$ for any d and $1\le k\le d$ for $1\le d\le 3$. The weight function for $k=2$ and $d=3$ was further simplified in Refs. [11, 26] as we will show in the Sec. VI B for general k and d.

B. Simplifying the integral over the intersection

The definition of the k-body weight function contains a cumbersome integral over the intersection of k surfaces. This integral can be simplified using

$$\int_{\partial B_1\cap\cdots\cap\partial B_k} f(\mathbf{r})\mathrm{d}^{d-k}\mathbf{r} = \int_{\mathbb{R}^d}[\mathbf{n}_1,\dots,\mathbf{n}_k]f(\mathbf{r})\prod_{i=1}^k w_{d-1}(\mathcal{B}_i,\mathbf{r})\mathrm{d}\mathbf{r} \quad (26)$$

for any function $f:\mathbb{R}^d\to\mathbb{R}$, see Refs. [11, 26] for $k=2$ and $d=3$ and Appendix A. Here, we used the subspace determinant, $[\mathbf{n}_1,\dots,\mathbf{n}_k]\equiv|\det(M)|$ (see page 598 in [35]), where M is the matrix M whose elements are $M_{i,j}=\mathbf{n}_i\cdot\mathbf{e}_j^N$ for $1\le i,j\le k$ expressed in some orthonormal basis $\mathbf{e}_j^N$ of the k-dimensional subspace spanned by the normal vectors. With this definition, all k-body weight functions have the form

$$w^{[k]}\big(\mathcal{B}_1,\dots,\mathcal{B}_k;\mathbf{r}\big)=Q_d^{[k]}(\mathcal{B}_1,\dots,\mathcal{B}_k;\mathbf{r})\prod_{i=1}^k w_{d-1}(\mathcal{B}_k,\mathbf{r}). \quad (27)$$

Here, the functions $Q_d^{[k]}$ do not contain any distributions unlike $w^{[k]}$ and only depend on the local properties of the surfaces ∂B_i at the intersection point $\mathbf{r}$. The $Q_d^{[k]}$ are summarized in Tbl. I.

VII. Fundamental mixed measure functional

Inserting the expression (19) for $\chi[\mathrm{St}_n(\mathbf{R}^n)]=\gamma(\mathrm{St}_n,\partial\mathrm{St}_n)$ into our approximation for the virial expansion of the excess free energy (12) and recalling Eqn. (14) for c_n , we find

$$\mathcal{F}_{\mathrm{exc}}=\int_{\mathbb{R}^d}\mathrm{d}\mathbf{r}\sum_{k=1}^d\Phi_d^{[k]}, \quad (28)$$

where

$$\Phi_d^{[k]}\equiv n^{[k]}(\mathbf{r})\sum_{n=k}^\infty\frac{k!}{n(n-1)}\binom{n}{k}n_d(\mathbf{r})^{n-k} = n^{[k]}(\mathbf{r})\chi_k\big(n_d(\mathbf{r})\big) \quad (29)$$

with

$$\chi_k(\eta)=\begin{cases}\partial^k[(1-\eta)\log(1-\eta)+\eta]/\partial\eta^k & \text{for } \eta<1 \text{ and}\\ \infty & \text{for } \eta\ge 1.\end{cases}$$

Here, the weighted density n_d is defined as usual, see Eqn. (5), while the k-body weighted density is defined as

$$n^{[k]}(\mathbf{r})\equiv\int_{\mathbb{V}^k}\mathrm{d}\mathbf{R}^k\,w_0^{[k]}(\mathbf{R}^k,\mathbf{r})\prod_{i=1}^k\rho(\mathbf{R}_i).$$

By integrating the k-body weight functions over all positions of the particles, we obtain mixed Minkowski volumes (or 'fundamental mixed measures'), which are generalizations of the fundamental measures to multiple

bodies [42]. Therefore, the DFT with the functional (28) could be called 'fundamental mixed measure theory' (FMMT). A FMMT functional containing only one-body and two-body weighted densities has already been derived from the lowest order virial order and applied to spherocylinders [43].

Note that the free energy is infinite if $n_d(\mathbf{r}) > 1$ for any $\mathbf{r}$. This is a physical divergence, as $n_d(\mathbf{r}) > 1$ implies that the point $\mathbf{r}$ lies inside more than one particle on average; therefore, some particles must overlap at $\mathbf{r}$ and the free energy should indeed be infinite.

We will now compare the FMMT functional to the exact result in the zero dimensional limit.

A. Comparison to the zero dimensional limit

Consider a mono-disperse system of hard particles in a quasi-zero-dimensional system, that is in a cavity that is so small that only one particle fits into the cavity. Alternatively, in a multi-component system an artificial external potential can be considered, which allows only particles of a single species to be inserted. Denote the accessible domain of the particle by $\mathbb{V}$, the set of coordinates $\mathbf{R}$ (positions and orientations) that the particle can have without extruding from the cavity. The set of accessible coordinates $\mathbb{V}$ is not necessarily connected as the cavity can have any shape.

The usual approach to obtain the free energy of this system starts with the grand canonical partition sum Ξ that can be calculated exactly for this quasi-zero-dimensional system, $\Xi = 1 + z|\mathbb{V}|$, where $z = \exp(\beta\mu)/\mathcal{V}$ is the fugacity and $|\mathbb{V}|$ is the accessible hyper-volume. From this, the excess free energy can be calculated [10],

$$\beta\mathcal{F}_{\text{exc}} = (1-x)\log(1-x) + x. \tag{30}$$

where $x = \langle N\rangle$ is the average number of particles in this system, which is less than one.

A second approach to obtain the excess free energy would be to perform a virial expansion for this system. For all configurations that contribute to a Mayer diagram, that is, for all configurations $\mathbf{R}^n \in \mathbb{V}^n$, each particle always overlaps with all other particles by construction. Therefore, each of the Mayer diagrams can be evaluated easily in this quasi-zero-dimensional system, as the Mayer bonds are always -1 and the density profile $\rho(\mathbf{R}) = \rho \equiv \langle N\rangle/|\mathbb{V}|$ is constant for all $\mathbf{R} \in \mathbb{V}$ (and $\rho(\mathbf{R}) = 0$ if $\mathbf{R} \notin \mathbb{V}$). The resulting value of a diagram g with n nodes and $|P(g)|$ bonds is

$$g = \frac{1}{|\text{Aut}(g)|}\int_{\mathbb{V}^n} \mathrm{d}\mathbf{R}^n\,(-1)^{|P(g)|}\rho^n = \frac{(-1)^{|P(g)|}}{|\text{Aut}(g)|}x^n. \tag{31}$$

Therefore, the virial result for the excess free energy (2) in this case is

$$\beta F_{\text{exc}} = -\sum_{n=2}^{\infty}\left[\sum_{g\in\mathcal{M}[n]}\frac{(-1)^{|P(g)|}}{|\text{Aut}(g)|}\right]x^n. \tag{32}$$

As before, we use the combinatorial result [25] $c_n \equiv -\sum_{g\in\mathcal{M}[n]}(-1)^{|P(g)|}/|\text{Aut}(g)| = 1/[n(n-1)]$ to obtain

$$\beta F_{\text{exc}} = \sum_{n=2}^{\infty}\frac{x^n}{n(n-1)} = (1-x)\log(1-x) + x, \tag{33}$$

which, of course, is equal to the exact excess free energy (30), as obtained from the partition sum.

A functional can be obtained using this system [10] by taking the zero-dimensional limit, $\mathbb{V} \to \{\mathbf{R}_i^{0\text{D}}\}$, where $\mathbf{R}_i^{0\text{D}}$ for $1 \le i \le M$ are the only accessible (discrete) states in the resulting 'zero-dimensional' cavity. In this limit, the density profile is simply a sum over delta functions and the functional can be constructed by demanding that the excess free energy from the functional goes to the exact free energy for this system (30) in the zero dimensional limit. For details on the calculation, see the original works for spheres [4, 10] and the extension to anisometric particles [27]. In two and three dimensions, the excess free energy from the functional could not be reduced to the exact expression (30) for cavities for which $\bigcap_{i=1}^{M}\mathcal{B}(\mathbf{R}_i^{0\text{D}})$ was empty. These cavities were subsequently ignored. The virial expansion route to the excess free energy in Eqns. (31)–(33) shows that (i) the resulting functional is equivalent to the one obtained in this work by performing a virial expansion and ignoring all n-particle configurations $\mathbf{R}^n$ for which $\bigcap_{i=1}^{M}\mathcal{B}(\mathbf{R}_i^{0\text{D}}) = \emptyset$ and (ii) the nontrivial combinatorial result $c_n = 1/[n(n-1)]$ can actually be obtained by considering the quasi-zero-dimensional system as the excess free energy (33) has to be exact in that system.

It should be noted that the final form for the functional proposed in Ref. [4] for hard spheres differs from the functional obtained in Sec. VII, as additional approximations were performed in Ref. [4] to obtain an efficient expression and the functional was rescaled to obtain a more accurate result for the homogeneous fluid. We outline these approximations in Sec. VII C.

B. Direct correlation function

One way to test the accuracy of the approximated functional is to compare the second direct correlation function

$$c(\mathbf{R}_1,\mathbf{R}_2) = -\beta\frac{\delta^2 F_{\text{exc}}}{\delta\rho(\mathbf{R}_1)\delta\rho(\mathbf{R}_2)} \tag{34}$$

with simulation results and established theories, which we will do in the following. Since previous results for $c(\mathbf{R}_1,\mathbf{R}_2)$ are only available for the homogeneous and isotropic bulk fluid (isotropic phase), we restrict ourselves to a constant density profile. In principle, we could obtain $c(\mathbf{R}_1,\mathbf{R}_2)$ by inserting the constant density profile into Eqn. (34) with the functional (28) and performing the many-particle integrals explicitly; however, we chose a simpler route using the kinematic formula from integral geometry (see below).

We start with Eqn. (12) for $\mathcal{F}_{\rm exc}$ in which the $\rho(\mathbf{R}_i)$ occur in an explicitly symmetric fashion, which makes it easier to perform the functional derivatives. Inserting Eqn. (12) in Eqn. (34) and using Eqn. (14) for c_n, we find that

$$c(\mathbf{R}_1,\mathbf{R}_2) = \\ -\sum_{n=2}^{\infty}\int_{\mathbb{V}^{n-2}}\mathrm{d}\mathbf{R}_3^n\,\chi\big[\bigcap_{i=1}^n\mathcal{B}(\mathbf{R}_i)\big]\prod_{i=3}^n\rho(\mathbf{R}_i), \quad (35)$$

where $\int_{\mathbb{V}^{n-k}}\mathrm{d}\mathbf{R}_{k+1}^n = \int_{\mathbb{V}}\mathrm{d}\mathbf{R}_{k+1}\cdots\int_{\mathbb{V}}\mathrm{d}\mathbf{R}_n$ and the prefactor $c_n = 1/(n(n-1))$ is cancelled by the factors $n(n-1)$ that appear in the second functional derivative of $\prod_{i=1}^n\rho(\mathbf{R}_i)$. From this expression, it can be seen that $c(\mathbf{R}_1,\mathbf{R}_2)$ only depends on the properties of $\mathcal{B}_{1\cap2}\equiv\mathcal{B}(\mathbf{R}_1)\cap\mathcal{B}(\mathbf{R}_2)$ and not on the properties of the separate particles. As a result, we can consider $\bigcap_{i=1}^n\mathcal{B}(\mathbf{R}_i)$ as the intersection of a fixed particle $\mathcal{B}_0\equiv\mathcal{B}_{1\cap2}$ and n' moving particles $\mathcal{B}_i=\mathcal{B}(\mathbf{R}_{i+2})$ for $1\le i\le n'$, where $n'=n-2$.

To calculate $c(\mathbf{R}_1,\mathbf{R}_2)$ for the isotropic and homogeneous fluid, we will use the iterated kinematic integral formula [35, Theorem 5.1.5] from integral geometry, which leads to Isihara's formula for the second virial coefficient [44] when restricted to the Euler characteristic and two convex particles in three dimensions. The iterated kinematic formula is also valid for quite general [45] classes of *non*-convex bodies $\mathcal{B}_i$ and for other intrinsic volumes than the Euler characteristic; however we only require the formula for the Euler characteristic, which reads

$$\int_{G_d^n}\mathrm{d}g^n\chi\big(\mathcal{B}_0\cap g_1\mathcal{B}_1\cap\cdots\cap g_n\mathcal{B}_n\big) \\ = \sum_{\substack{i_0,\cdots,i_n=0\\ i_0+\cdots+i_n=nd}}^{d} C_{i_0,\cdots,i_n}v_{i_0}(\mathcal{B}_0)\cdots v_{i_n}(\mathcal{B}_n), \quad (36)$$

where $\int_{G_d^n}\mathrm{d}g^n\equiv\int_{G_d}\mathrm{d}g_1\cdots\int_{G_d}\mathrm{d}g_n$ denotes the n-fold integral over G_d, the group of rigid body motions (translations and rotations) isomorphic to $\mathbb{R}^d\times\mathbb{SO}(d)$, normalized such that $\int_{G_d}\mathrm{d}g\,w_d(g\mathcal{B},\mathbf{r}) = v_d(\mathcal{B})$; also, $v_i(\mathcal{B}_j)$ is the ith intrinsic volume of body $\mathcal{B}_j$ (for $d=3$, v_0, πv_1, $2v_2$ and v_3 are the Euler characteristic, the integrated mean curvature, the surface area and the volume respectively) and, finally, $C_{i_0,\cdots,i_n}$ is a prefactor,

$$C_{i_0,\cdots,i_n}\equiv i_0!\kappa_{i_0}\prod_{j=1}^n\frac{i_j!\kappa_{i_j}}{d!\kappa_d}$$

with κ_i the volume of the i-dimensional unit ball B_i (*i.e.* the solid sphere with unit radius). For bodies with a smooth boundary, the intrinsic volumes v_i for $1\le i\le d-1$ can be calculated using [35, Page 607]:

$$v_i(\mathcal{B})\equiv\frac{\binom{d}{i}}{d\kappa_{d-i}}\int_{\partial\mathcal{B}}\mathrm{d}^{d-1}\mathbf{r}\,H_{d-i-1}(\mathcal{B},\mathbf{r}), \quad (37)$$

where $H_0=1$ and H_j is the product of j principal curvatures averaged over all combinations of j principal directions:

$$H_j(\mathcal{B},\mathbf{r}) = \binom{d-1}{j}^{-1}\sum_{i_1,\cdots,i_j=0}^{d-1}\prod_{k=1}^{j}\kappa_{i_j}(\mathcal{B},\mathbf{r}),$$

Also, we denote the volume of a body $\mathcal{B}$ by $v_d(\mathcal{B})$. In principle, it should be possible to prove the kinematic formula, which is outside of the scope of this work, by inserting $\chi(\mathrm{St}_n)=\gamma(\mathrm{St}_n,\mathbb{R}^n)$ from Eqn. (19) and performing the integrals over $\mathbf{R}_j$ for $1\le j\le n$ and $\mathbf{r}$.

While the iterated kinematic formula looks complicated for large n, it should be realized that due to the condition $i_0+\cdots+i_n=nd\Leftrightarrow\sum_{j=1}^n(d-i_j)=i_0$ only at most i_0 of the i_j for $1\le j\le n$ are unequal to d, such that the factors in $C_{i_0,\cdots,i_n}$ corresponding to the remaining i_j are unity.

In order to write the direct correlation function (35) for the bulk fluid in the form of the iterated kinematic formula, we rewrite the combined integral and sum over the (generalized) coordinate $\mathbf{R}_j$ in Eqn. (35) as

$$\int_{\mathbb{V}}\mathrm{d}\mathbf{R}_j\,\rho(\mathbf{R}_j)\chi(\mathcal{B}(\mathbf{R}_j)\cap\cdots) = \\ \sum_{s_j=1}^{M}\int_{G_d}\mathrm{d}g_j\,\bar\rho_{s_j}\,\chi(g_j\mathcal{B}_{s_j}^{(0)}\cap\cdots),$$

for a constant density profile $\rho(\mathbf{R})=\bar\rho_s/|\mathbb{SO}(d)|$, where M is the number of species in the system, $\mathcal{B}_s^{(0)}$ is the set of points inside a particle of species s centered at the origin with identity orientation, (see also Sec. II) and $|\mathbb{SO}(d)|=\int_{\mathbb{SO}(d)}\mathrm{d}\mathcal{R}$ the volume of the group of rotations in Eqn. (35). Now we can apply the iterated kinematic formula, and subsequently simplify the resulting expression by denoting the number of i_j's equal to α by N_α for $0\le j\le n$ and $k=\sum_{\alpha=0}^{d-1}N_\alpha$ is the number of i_j's unequal to d. Also we define the scalar (one-body) weighted densities

$$\tilde n_i = \frac{i!\kappa_i}{d!\kappa_d}\sum_{s=1}^{M}v_i(\mathcal{B}_s^{(0)})\bar\rho_s$$

(note that $\tilde n_d=\eta$ is the packing fraction), which are normalized differently than the n_A from FMT for $d=3$. With these definitions, the direct correlation func-

tion (35) becomes

$$c(\mathbf{R}_1,\mathbf{R}_2) = -\sum_{n'=0}^{\infty}\sum_{i_0=0}^{d} i_0!\kappa_{i0}\, v_{i_0}(\mathcal{B}_{1\cap2}) \sum_{\substack{N_0,N_1,\dots,N_{d-1}\geq 0\\ dN_0+(d-1)N_1+\cdots+1N_{d-1}=i_0}} \tilde{n}_0^{N_0}\tilde{n}_1^{N_1}\cdots\tilde{n}_{d-1}^{N_{d-1}} \sum_{N_d\geq 0}\delta_{N_0+\cdots+N_d,n'}\frac{n'!}{N_0!N_1!\cdots N_d!}\eta^{N_d}$$
$$= -\sum_{i_0=0}^{d} v_{i_0}(\mathcal{B}_{1\cap2})\sum_{k=0}^{i_0} c_{i_0}^{[k]}(\tilde{n}_0,\cdots,\tilde{n}_{d-1})\,\chi_{k+2}(\eta) \tag{38}$$

where we used that the number of combinations of i_j for $0\leq i\leq n'$ that lead to the same N_α factors $\tilde{n}_\alpha$ for $0\leq\alpha\leq d$ is given by $n'!/(N_0!\cdots N_d!)$ and we defined

$$c_{i_0}^{[k]} = i_0!\kappa_{i0} \sum_{\substack{N_0,N_1,\dots,N_{d-1}\geq 0\\ N_0+N_1+\cdots+N_{d-1}=k\\ dN_0+(d-1)N_1+\cdots+1N_{d-1}=i_0}} \frac{\tilde{n}_0^{N_0}}{N_0!}\cdots\frac{\tilde{n}_{d-1}^{N_{d-1}}}{N_{d-1}!}.$$

Note that the latter sum contains only very few terms for low d (at most one for $d=2,3$).

Now we will compare to available expressions from different theories and simulation results for the direct correlation function to assess the accuracy of the functional. The virial series up to first order in density for general shapes and general d reads

$$c_{\text{exact}}(\mathbf{R}_1,\mathbf{R}_2) = f_M(\mathbf{R}_1,\mathbf{R}_2) + \text{} + \cdots$$

where  denotes

$$f_M(\mathbf{R}_1,\mathbf{R}_2)\int_{\mathbb{V}} \mathrm{d}\mathbf{R}_3\,\rho(\mathbf{R}_3)\,f_M(\mathbf{R}_2,\mathbf{R}_3)f_M(\mathbf{R}_3,\mathbf{R}_1).$$

We see that the lowest order is satisfied by the FMMT approximation for $c(\mathbf{R}_1,\mathbf{R}_2)$ as $f_M(\mathbf{R}_1,\mathbf{R}_2) = -\chi\big(\mathcal{B}(\mathbf{R}_1)\cap\mathcal{B}(\mathbf{R}_2)\big)$ and $c_0^{[0]}=1$. In order to consider the first order in density, we have to connect the integrals in  to geometry. It is relatively easy to see [46][45, Eqn. (46)] that $(\mathcal{B}(\mathbf{R}_i)-\mathcal{R}\mathcal{B}_s^{(0)})$ is the region excluded for the center of $\mathcal{R}\mathcal{B}_s^{(0)}$ by $\mathcal{B}(\mathbf{R}_i)$, where $\mathcal{A}-\mathcal{B}=\{\,a-b\,|\,a\in\mathcal{A}\text{ and }b\in\mathcal{B}\,\}$ for two bodies $\mathcal{A}$ and $\mathcal{B}$. Therefore, the positional integral in $-$, whose integrand is nonzero if $\mathcal{R}_3\mathcal{B}_s^{(0)}+\mathbf{r}_3$ overlaps with both $\mathcal{B}(\mathbf{R}_1)$ and $\mathcal{B}(\mathbf{R}_2)$, can be written as the volume of $(\mathcal{B}(\mathbf{R}_1)-\mathcal{R}_3\mathcal{B}_s^{(0)})\cap(\mathcal{B}(\mathbf{R}_2)-\mathcal{R}_3\mathcal{B}_s^{(0)})$ [47]. The geometry of this region is different from the excluded region of $\mathcal{R}_3\mathcal{B}_s^{(0)}$ and $\mathcal{B}_{1\cap2}$, which is the corresponding result from FMMT, due to lost cases. As a result, no amount of rescaling can fix this difference once and for all for general (mixtures of) shapes. Nevertheless, for particular shapes (see Sec. VII C), the difference may be small or indeed zero.

In order to make this difference in geometries more explicit and examine effects of higher densities, we turn to the bulk hard sphere fluid and compare to the Percus-Yevick (PY) direct correlation function [49]. The FMMT $c(\mathbf{R}_1,\mathbf{R}_2)$ was calculated using Eqn. (38) and the intrinsic volumes $v_i(\mathcal{B}_{1\cap2})$ of the intersection of two spheres using Eqn. (37) and $v_i(\mathcal{B}_{1\cap2}) = \lim_{\epsilon\to0} v_i\big((\mathcal{B}_{1\cap2})_\epsilon\big)$, see Eqn. (25) for the definition of the parallel body $(\cdot)_\epsilon$ and Refs. [16, 17] for a similar procedure. For hard spheres, all $v_i(\mathcal{B}_{1\cap2})$ are polynomials in the distance r between the centers of $\mathcal{B}(\mathbf{R}_1)$ and $\mathcal{B}(\mathbf{R}_2)$ except for $v_1(\mathcal{B}_{1\cap2})$, which is proportional to the mean half width or the integrated mean curvature and contains a term proportional to $\arcsin(r/\sigma)\sqrt{\sigma-r^2}$, where σ is the hard sphere diameter. However, the first order exact contribution $-$ is the volume of the intersection between two spheres with diameter 2σ at a center-to-center distance r, which is a polynomial in r only. So we again see that rescaling will not make the FMMT and exact first order contributions in $c(r,\eta)$ agree for all r and η. Nevertheless, the difference between the exact and the FMMT approach might still be numerically small in practice. To access this difference, we compare the direct correlation function from FMMT to the ones from PY and simulations in Fig. 5. We see that the deviation of FMMT from the simulation results [48] is larger than for PY; however, the FMMT direct correlation function never performs more than an order of magnitude worse than the PY $c(\mathbf{R}_1,\mathbf{R}_2)$. We also show the three direct correlation functions as a function of η at $r=0$ (where lost cases do not contribute to the triangle diagram) to show that the lost cases in  are not the only cause for the difference between the PY

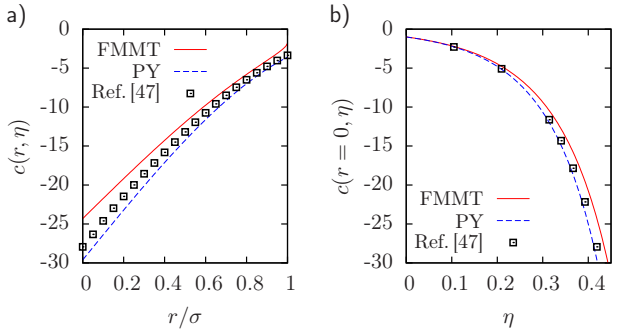


FIG. 5. (a) The direct correlation function from FMMT, see Eqn. (38), at $6\eta/\pi=0.8$ compared to the Percus-Yevick $c(r,\eta)$ (PY) and simulation results by Groot, Eerden and Faber [48]. (b) The behavior of the FMMT direct correlation function with varying η at $r=0$, where lost cases do not contribute to first order in η, is compared with the Percus-Yevick result. As the lost cases do not contribute here, the first order in η of the FMMT $c(r,\eta)$ is exact (as is the first order PY result).

and FMMT predictions for $c(r, \eta)$.

We will now review the methods that have been used in the literature to overcome these difficulties for hard spheres.

C. Expansion and rescaling

First, the equation of state for the homogeneous fluid from the functional from Sec. VII is not very accurate. Because of the neglected lost cases, the density expansion of the FMT free energy is already inexact at the third virial order. This is especially pronounced for thin rods, where a significant contribution of the exact triangle diagram is due to lost cases where the three particles are nearly coplanar and the three regions of pairwise intersection are well-separated. This effect of lost cases becomes especially problematic in two dimensions, where any FMT-like functional would incorrectly predict a vanishing third virial coefficient for infinitely thin needles. This same problem would also occur in a highly ordered uni-axial nematic phase of biaxial platelets (when the particle is very thin along one of its axes) [50]. On the other hand, the FMMT functional for hard parallel cubes, which is equal to Cuesta's functional [20], is exact at the third virial order because there are no lost cases for hard cubes. In fact, this also holds independently of the edge-lengths for (mixtures of) other single-orientation parallelepipeds and their d-dimensional generalizations with $2d$ facets, provided that each facet of each species is perpendicular to one of d linearly independent directions $\mathbf{u}_i$ [51].

In Ref. [4], as well as in the original derivation of FMT by Rosenfeld [3], the $\Phi_3^{[3]}$ term in the functional for hard spheres was rescaled to obtain the exact third virial coefficient. For anisotropic particles, the prefactor of $\Phi_3^{[3]}$ is either kept equal to that of spheres [11] or it is modified [14] such that the correct third virial coefficient for anisotropic particles is obtained (the third virial coefficient has to be calculated numerically in general).

Secondly, the generalized weighted densities $n_0^{[k]}$ contain k integrals over the particles' coordinates, such that calculating these directly is computationally involved for $k > 1$ and $d > 2$ [52]. An efficient functional can be obtained if the generalized weighted densities for $k \geq 2$ are expanded in products of k single-particle weight functions. Using a similar calculation as Wertheim's deconvolution of the Mayer bond [26], the $n^{[2]}$ weighted density in three dimensions can be expanded in either tensor weighted densities (that is weighted densities that transform as tensors under a rotation of the basis vectors) or weighted densities that transform as the spherical harmonics under a rotation of the basis vectors.

For the kernel of the third term, $Q_3^{[3]}$, Tarazona and Rosenfeld's approximation [4] for hard spheres can be reinterpreted as the geometrical approximation shown in Fig. 6. In this approximation, we first write the area of

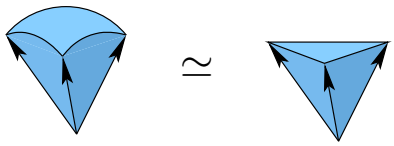


FIG. 6. The geometrical consideration behind the approximation (39) for the third term in the three dimensional FMT functional.

the spherical triangle spanned by three normal vectors $\mathbf{n}_i$ at a point $\mathbf{p}$ on a triple surface intersection as three times the volume of the corresponding section of a unit ball. Subsequently, we replace the volume of this section of the unit ball by the volume of a tetrahedron that has the normal vectors as three of its edges, $\frac{1}{6}|\mathbf{n}_1 \cdot (\mathbf{n}_2 \times \mathbf{n}_3)|$. The final form for the approximation then reads $\sigma_2\big(N^+(\mathrm{St}_n, \mathbf{p})\big) \simeq \frac{1}{2}|\mathbf{n}_1 \cdot (\mathbf{n}_2 \times \mathbf{n}_3)|$, such that the kernel becomes

$$Q_3^{[3]} \simeq \frac{1}{48\pi}[\mathbf{n}_1 \cdot (\mathbf{n}_2 \times \mathbf{n}_3)]^2 \tag{39}$$

for general shapes. This approximation is exact in the limit that the density profile goes to a single infinitely sharp peak centered around some position and orientation.

Approximations for $n^{[k]}$ have to be formulated with some care, because otherwise some of the important properties of the generalized weight function might be lost. For instance, the exact $Q_d^{[k]}$ for $k \geq 2$ vanishes if one of the particles i is moved on top of another particle j, $\lim_{\mathbf{R}_i \to \mathbf{R}_j} Q_d^{[k]}(\mathbf{R}^k, \mathbf{r}) = 0$, due to the prefactor $[\mathbf{n}_1, \cdots, \mathbf{n}_k]$ and, at least for $k = d = 3$, it is important [4, 5] that the approximation for $Q_3^{[3]}$ also vanishes in this limit. Failing to take this condition into account causes a negative divergence in the zero dimensional limit for hard spheres [10] and causes the crystal to be unstable with respect to the fluid for the whole density range.

After the expansion was performed for hard spheres, the third term in the functional for $d = 3$ was rescaled to obtain the correct third virial coefficient for hard spheres [4], which leads to the PY equation of state (via the compressibility route). The kernel $Q_3^{[3]}$ has also been modified by Tarazona [5] to obtain the exact triangle diagram in the direct correlation function for the homogeneous fluid of hard spheres. The latter calculation results, without further modifications, in the Percus-Yevick direct correlation function for spheres [49].

Finally, we have made approximations beyond just neglecting the lost cases: we ignored all Ree-Hoover diagrams other than $(\emptyset)_n$. These can be taken into account approximately for the homogeneous fluid by adapting the functional to fit some equation of state (EOS), which is then an input for the theory rather than a result. The modifications proposed by Roth *et al* [6, 7], multiplying each term $\Phi_d^{[k]}$ by a certain function of $n_d(\mathbf{r})$ only, lead to the so-called White Bear II functional, which is still

accurate for the crystal and results by construction in the highly accurate Carnahan Starling equation of state for the homogeneous fluid of spheres. Note, that semi-empirical modifications that improve the EOS of the fluid for specific shapes do not necessarily improve the results for strongly inhomogeneous and/or anisotropic density profiles and that the White-Bear II functional is only accurate for moderately non-spherical shapes even in the homogeneous case [47, 53].

VIII. Summary and discussion

We have derived a density functional from an approximated and resummed virial expansion for hard particles with arbitrary convex shapes in $1 \leq d \leq 3$ dimensions. While all Mayer diagrams were considered, we approximated each diagram by neglecting those configurations for which the intersection between all particles was empty. This is the only approximation in our derivation. All approximated n-particle diagrams become proportional to the same integral, while the sum of the prefactors could be obtained by comparing to Ree and Hoover's resummation of the Mayer diagrams [25]. Using the geometry of the n-particle intersection, we wrote the approximated Mayer diagrams in terms of generalized, k-body weight functions and resummed the series to a closed form containing d terms in $1 \leq d \leq 3$ spatial dimensions. The resulting functional equals the fundamenal measure functional (0D-FMT) that was earlier derived from consideration of an extremely confined geometry (the 'zero-dimensional limit'), which tells us that the virial series is actually contained, in an approximate sense, in the previously proposed FMT functionals.

The geometric formulation of the resulting functional has the advantage that results from integral geometry can be directly transfered to 0D-FMT, which we used to calculate the direct correlation function for constant densities. We showed that the direct correlation function thus obtained has a different geometrical origin than the exact virial expansion for general shapes already at the $\propto \rho$ term. A similar fundamental difference in form is also found when comparing the 0D-FMT result to the established Percus-Yevick (PY) result for hard spheres at finite density, although, in practice, the accuracy of 0D-FMT turns out to be mostly comparable to that of PY for the direct correlation function at high densities.

The generalized weight functions in 0D-FMT contain integrals over the coordinates of $1 \leq k \leq d$ particles. To simplify the generalized weight functions, they can be expanded into one-body weight functions. We briefly reviewed the possibilities to perform this expansion as proposed in Refs. [4, 5, 11, 26] and reiterated the conditions for this expansion to yield a functional for a given d that correctly reduces to the functional for $d' < d$ when applied to a system under strong confinement. Correct behavior under such dimensional reduction has turned out to be important for the crystal of hard spheres [5, 10].

The success of FMT for spheres is perhaps unexpected considering the severity of our approximation and the ones that were made afterwards [4, 5]. The effect of our approximation becomes more clear if Ree and Hoover's resummation of the Mayer diagrams into a sum of other types of diagrams [25] is considered. We showed that neglecting all configurations with an empty St_n in the n-particle Mayer diagrams is equivalent to the following two approximations on the Ree-Hoover diagrams: First, we neglect all n-particle Ree-Hoover diagrams but $(\emptyset)_n$, the Ree-Hoover diagram where each particle is required to overlap with all other particles. Subsequently, the $(\emptyset)_n$ diagram is approximated by neglecting the 'lost cases' [4], which are configurations for which each particle overlaps with all other particles, but there is no common region of overlap ($\mathrm{St}_n = \emptyset$). The former approximation would lead to an overestimation of the free energy, at least for the bulk fluid of hard spheres [25, 31], as the neglected e_{RH}-bonded Ree-Hoover diagrams sum up to a net negative contribution. The latter approximation, neglecting the lost cases, leads to an underestimation of the $(\emptyset)_n$ diagram (both the exact and approximated $(\emptyset)_n$ diagrams are positive if the combinatorial prefactors are included) even after rescaling to obtain the correct third order diagram; therefore, the approximation lowers the free energy. The effect of these two approximations cancels partially for hard spheres and probably also for other shapes, which might explain FMT's success. As mentioned in Sec. VII C, particles like hard cubes have no lost cases, such that no partial cancellation occurs. Nevertheless, the phase behavior of hard parallel cubes is described reasonably well by Cuesta and Martínez-Ratón's FMT functional [54, 55].

We note that our functional for $d = 1$ agrees with the exact functional for inhomogeneous hard-rod mixtures that was derived by Vanderlick, Davis and Percus [56]. In $d = 1$ dimensions, there are no lost cases for hard rods [57], so the $(\emptyset_n)$ diagram is exactly contained in our functional. Therefore, we have proven that only the $(\emptyset_n)$ Ree-Hoover diagrams contribute for hard rods for $d = 1$ for any density profile, which was shown before for homogeneous systems and conjectured to be true for inhomogeneous density profiles [25]. As mentioned before, the success of a functional for crystallization is highly dependent on the behavior under dimensional reduction. As our functional and the other modern FMT functionals for $d > 1$ by construction reduce to the $d = 1$ case under confinement in the narrowest possible (straight) channel, this might also explain some of the successes of the functional.

Finally, one of the requirements that allowed Rosenfeld to derive FMT is that FMT obeys the scaled particle relation, *i.e.* the excess chemical potential for adding a large particle to the mixture becomes equal to work against pressure required to clear a region of the size of the particle in the limit when the particle becomes macroscopically large. The version from the zero-dimensional limit and the other versions of FMT exhibit the correct scaled

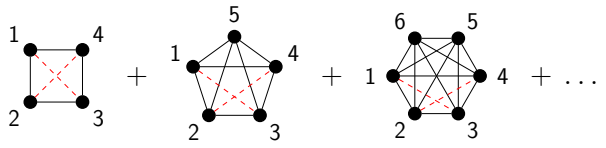


FIG. 7. The next diagrams in the Ree-Hoover resummation, if the diagrams are added in order of increasing number of e_{RH}-bonds (dashed lines) or, equivalently, decreasing number of f_M bonds (solid lines). The sign and combinatorial prefactor [25] are contained in the diagram.

particle limit, which probably also adds to the accuracy of the functional.

Now, we are able to discuss possible improvements beyond the current functional. The first and most obvious improvement would be to include the 'lost cases'. Wertheim has shown how , the lowest-order Mayer diagram that suffers from lost cases, can be written in terms of two-center weighted densities, that is, generalized weighted densities that depend on two positions. Future improvements should probably include these two-center weighted densities, as the lost cases cannot be recovered for a general density profile if only one-center weighted densities are used.

Secondly, other Ree-Hoover diagrams might be added to the functional, and (after suitable approximation) be written in terms of two-center weighted densities. For hard spheres, for example, Ree and Hoover [31] noted that the n-particle diagrams in the virial expansion for the homogeneous fluid could be approximated reasonably well for $n \leq 7$ by including only the $(\emptyset)_n$ diagram and the diagram with two e_{RH} bonds, see Fig. 7. After suitable labeling, the integrand in the latter diagram is nonzero if all pairs overlap except $(1,3)$ and $(2,4)$. In Ref. [39], several functionals containing multiple-center weighted densities are derived from the Ree-Hoover diagrams.

Finally, we could consider adding the Mayer ring diagrams, in which each particle i is only connected by a Mayer bond to two other particles, for example  and  are the ring diagrams with three and four particles, respectively. Due to the loose connectivity, this diagram can be evaluated with relative ease for the homogeneous fluid [58] and can be expressed in terms of Wertheim's two-center weighted densities [26]. It would be interesting to consider replacing our approximations for the ring diagrams (and similar loosely connected diagrams) by their exact values and see if this leads to an improvement of the functional.

Acknowledgments

The idea for this paper originated during a visit of MM and SK to Martin Oettel in Tübingen. We would like to thank Martin Oettel, Roland Roth and others present at the time for fruitful discussions. Financial support by the DFG under grant Me1361/12 as part of the Research Unit 'Geometry and Physics of Spatial Random Systems' is gratefully acknowledged by KM, while SK was supported by the Cluster of Excellence "Tailor-Made Fuels from Biomass", funded by the Excellence Initiative of the German federal and state governments.

A. Appendix: intersections of delta shells

In this section, we will derive Eqn. (26), which is a generalization of the results for $k = 2$ [11] and $k = 3$ [22] in $d = 3$ dimensions. Consider the parallel body of the intersection between k-surfaces $\partial\mathcal{B}_i$, $(\Sigma_k)_\epsilon \equiv (\partial\mathcal{B}_1 \cap \cdots \cap \partial\mathcal{B}_k)_\epsilon$ and let $\mathcal{N}(\mathbf{p})$ be the k-dimensional subspace spanned by the normal vectors of the intersecting surface at $\mathbf{p}$. The integrand on the right hand side of Eqn. (26) is zero if $\mathbf{r} \notin (\Sigma_k)_\epsilon$ for some ϵ, such that the right hand side of Eqn. (26) becomes

$$\int_{(\Sigma_k)_\epsilon} \mathrm{d}\mathbf{r}\, h(\mathbf{r}) \prod_{i=1}^{k} w_{d-1}(\mathcal{B}_i, \mathbf{r}),$$

where $h(\mathbf{r}) = f(\mathbf{r})[\mathbf{n}_1, \ldots, \mathbf{n}_k]$. Also, if ϵ is small enough, we can locally approximate $(\Sigma_k)_\epsilon$ as the parallel body of a flat $d-k$ dimensional plane, which allows us to approximate $(\Sigma_k)_\epsilon$ as $\{\mathbf{p}+\mathbf{x} | \mathbf{p} \in \Sigma_k,\ \mathbf{x} \in \mathcal{E}_\epsilon(\mathbf{p})\}$, where $\mathcal{E}_\epsilon(\mathbf{p})$ consists of those elements $\mathbf{r}$ of $\mathcal{N}(\mathbf{p})$ such that $|\mathbf{r}| < \epsilon$. With this approximation (which is exact in the limit $\epsilon \to 0$), we can write the right hand side of Eqn. (26) as

$$\lim_{\epsilon\to 0} \int_{\Sigma_k} \mathrm{d}^{d-k}\mathbf{p} \int_{\mathcal{E}_\epsilon(\mathbf{p})} \mathrm{d}\mathbf{x}\, h(\mathbf{p}+\mathbf{x}) \prod_{i=1}^{k} \delta\big(\mathbf{x}\cdot\mathbf{n}_i(\mathbf{p})\big),$$

where we locally approximated Σ_k as the intersection of k flat surfaces with normal vectors $\mathbf{n}_i(\mathbf{p})$. Now we parametrize $\mathbf{x} = \sum_{i=1}^{k} x_i \mathbf{e}_i^N$, where the $\mathbf{e}_i^N$ form an orthonormal basis of $\mathcal{N}(\mathbf{p})$ and perform the variable transformation $(x_1, \ldots, x_k) \to \mathbf{t}$, where $t_i = \mathbf{x}\cdot\mathbf{n}_i(\mathbf{p})$ is the argument of the ith delta function in the expression above for $1 \leq i \leq k$. The Jacobian matrix of the *inverse* transformation $\mathbf{t} \to (x_1, \ldots, x_k)$ has components $M_{ij} = \partial t_i/\partial x_j = \mathbf{n}_i(\mathbf{p})\cdot\mathbf{e}_j^N$, such that the Jacobian determinant of $(x_1, \ldots, x_k) \to \mathbf{t}$ equals $1/|\det(M)| = 1/[\mathbf{n}_1, \ldots, \mathbf{n}_k]$. After performing the variable substitution $(x_1, \ldots, x_k) \to \mathbf{t}$ and the integrals over the t_i, we obtain the left hand side of Eqn. (26), which completes the proof.

[1] S. Sacanna and D. J. Pine, Curr. Opin. Colloid. In. **16**, 96 (2011).
[2] R. Evans, Adv. Phys. **28**, 143 (1979).
[3] Y. Rosenfeld, Phys. Rev. Lett. **63**, 980 (1989).
[4] P. Tarazona and Y. Rosenfeld, Phys. Rev. E **55**, R4873 (1997).
[5] P. Tarazona, Phys. Rev. Lett. **84**, 694 (2000).
[6] R. Roth, R. Evans, A. Lang, and G. Kahl, J. Phys. Cond. Matt. **14**, 12063 (2002).
[7] H. Hansen-Goos and R. Roth, J. Phys. Cond. Matt. **18**, 8413 (2006).
[8] M. Oettel, S. Görig, A. Härtel, H. Löwen, M. Radu, and T. Schilling, Phys. Rev. E **82**, 051404 (2010).
[9] A. Härtel, M. Oettel, R. E. Rozas, S. U. Egelhaaf, J. Horbach, and H. Löwen, Phys. Rev. Lett. **108**, 226101 (2012).
[10] Y. Rosenfeld, M. Schmidt, H. Löwen, and P. Tarazona, J. Phys. Cond. Matt. **8**, L577 (1996).
[11] H. Hansen-Goos and K. Mecke, J. Phys. Cond. Matt. **22**, 364107 (2010).
[12] H. Hansen-Goos and K. Mecke, Phys. Rev. Lett. **102**, 018302 (2009).
[13] For a similar and earlier calculation, see M. S. Wertheim, Mol. Phys. **83**, 519 (1994).
[14] M. Marechal, U. Zimmermann, and H. Löwen, J. Chem. Phys. **136**, 144506 (2012).
[15] R. Wittmann and K. Mecke, J. Chem. Phys. **140**, 104703 (2014).
[16] M. Marechal, H. H. Goetzke, A. Härtel, and H. Löwen, J. Chem. Phys. **135**, 234510 (2011).
[17] M. Marechal and H. Löwen, Phys. Rev. Lett. **110**, 137801 (2013).
[18] M. Schmidt, Phys. Rev. E **63**, 050201 (2001).
[19] A. Esztermann, H. Reich, and M. Schmidt, Phys. Rev. E **73**, 011409 (2006).
[20] J. A. Cuesta and Y. Martínez-Ratón, Phys. Rev. Lett. **78**, 3681 (1997).
[21] Y. Martínez-Ratón, J. A. Capitán, and J. A. Cuesta, Phys. Rev. E **77**, 051205 (2008).
[22] S. Korden, Phys. Rev. E **85**, 041150 (2012).
[23] E. C. Oğuz, M. Marechal, F. Ramiro-Manzano, I. Rodriguez, R. Messina, F. J. Meseguer, and H. Löwen, Phys. Rev. Lett. **109**, 218301 (2012).
[24] Y. Rosenfeld, M. Schmidt, H. Löwen, and P. Tarazona, Phys. Rev. E **55**, 4245 (1997).
[25] F. H. Ree and W. G. Hoover, J. Chem. Phys. **40**, 939 (1964).
[26] M. S. Wertheim, Mol. Phys. **83**, 519 (1994), *ibid.* **89**, 989 (1996); *ibid.* **89**, 1005 (1996).
[27] M. Marechal, H. H. Goetzke, A. Härtel, and H. Löwen, J. Chem. Phys. **135**, 234510 (2011), App. B.
[28] J. P. Hansen and I. R. MacDonald, *Theory of simple liquids* (Academic Press, London, 1976) In the third edition, the equivalent expression for $c^{(1)} = -\beta\delta\mathcal{F}_{\rm exc}/\delta\rho(\mathbf{R})$ is given in Eq. (3.8.6).
[29] T. Morita and K. Hiroike, Progress of Theoretical Physics **25**, 537 (1961).
[30] Between each pair of nodes in a biconnected graph there are at least two paths of lines, such that each node occurs at most once on each path. Equivalently, a biconnected graph cannot be turned into a disconnected one by removing one node and all incident edges/lines.
[31] F. H. Ree and W. G. Hoover, J. Chem. Phys. **46**, 4181 (1967).
[32] J. R. J. Riddell and G. E. Uhlenbeck, J. Chem. Phys. **21**, 2056 (1953).
[33] F. H. Ree and W. G. Hoover, J. Chem. Phys. **41**, 1635 (1964).
[34] A. Kaouche and P. Leroux, Séminaire Lotharingien de Combinatoire **61**, B61Af (2009).
[35] R. Schneider and W. Weil, *Stochastic and integral geometry* (Springer, 2008).
[36] M. Moszyńska, *Selected topics in convex geometry* (Birkhäuser, Boston, 2006).
[37] The number m can be less than $\min\{n, d\}$, if one or more of the bodies lie inside other bodies in the stack.
[38] See *e.g.* K. Mecke, Journal of Statistical Physics **102**, 1343 (2001).
[39] S. Korden, "Density Functional Theory for Hard Particles in N Dimensions," (2014), arXiv:1403.2054 [cond-mat.soft].
[40] R. Schneider, Annali di Matematica Pura ed Applicata **116**, 101 (1978).
[41] S. Chern, American Journal of Mathematics **74**, pp. 227 (1952).
[42] H. Minkowski, Mathematische Annalen **57**, 447 (1903), 10.1007/BF01445180.
[43] R. Wittmann, M. Marechal, and K. Mecke, "Fundamental mixed measure theory," In preparation.
[44] A. Isihara, J. Chem. Phys. **18**, 1446 (1950).
[45] R. Schneider, in *Stochastic Geometry*, Lecture Notes in Mathematics, Vol. 1892, edited by W. Weil (Springer Berlin Heidelberg, 2007) pp. 119–184.
[46] B. M. Mulder, Mol. Phys. **103**, 1411 (20 May 2005).
[47] Y. Rosenfeld, J. Chem. Phys. **89**, 4272 (1988).
[48] R. D. Groot, J. P. van der Eerden, and N. M. Faber, J. Chem. Phys. **87**, 2263 (1987).
[49] M. S. Wertheim, Phys. Rev. Lett. **10**, 321 (1963).
[50] The same prediction results from the Zwanzig model in FMT, where each of the particle axes lies along one of the Cartesian axes; however, the *exact* third order virial coefficient also vanishes in that case.
[51] Define a non-orthogonal basis $\mathbf{e}_i$ of $\mathbb{R}^d$ by $\mathbf{e}_i \cdot \mathbf{n}_j = 0$ for all $i \neq j$. All positions can be uniquely decomposed in components r_j: $\mathbf{r} = \sum_{i=1}^{d} r_j \mathbf{e}_i$. For each particle i in a configuration, d intervals $[a_j^{(i)}, b_j^{(i)}]$ can be defined such that a point $\mathbf{r}$ lies in the interior of particle i if and only if $a_j^{(i)} \leq r_j \leq b_j^{(i)}$ for all $1 \leq j \leq d$. By the argument in footnote [57], there are no lost cases.
[52] Evaluating $n^{[k]}(\mathbf{r})$ once for every position for a density profile where all of the $d(d-1)/2$ orientational and d positional degrees of freedom are discretized on a grid of size G for all M species requires $G^d \left(M\, G^{d-1+d(d-1)/2}\right)^k$ evaluations of $Q_d^{[k]}$; for $d = k = 3$, $M = 1$ and a grid size of $G = 10^n$ this corresponds to 10^{13n} evaluations.
[53] R. Wittmann, M. Marechal, and K. Mecke, J. Chem. Phys. (2014), *in press*.
[54] J. A. Cuesta and Y. Martínez-Ratón, J. Chem. Phys. **107**, 6379 (1997).
[55] Y. Martínez-Ratón and J. A. Cuesta, J. Chem. Phys. **111**, 317 (1999).

[56] T. K. Vanderlick, H. T. Davis, and J. K. Percus, J. Chem. Phys. **91**, 7136 (1989).

[57] Sort the k line intervals, $[a_i, b_i]$, such that $a_1 < a_2 < \ldots < a_k$. If all of the intervals overlap pairwise, then $a_k < b_j$ for $j < k$. Since also $a_k > a_j$ for $j < k$, this implies that all intervals contain a_k, such that $\bigcap_{i=1}^{k} [a_i, b_i] \neq \emptyset$.

[58] E. W. Montroll and J. E. Mayer, J. Chem. Phys. **9**, 626 (1941).